Reevaluation of Piezo1 as a gut RNA sensor

Nickolls AR[1], O'Brien GS[1], Shnayder S[1], Zhang Y[2], Nagel M[1], Patapoutian A[2], Chesler AT[1,*]

[1]National Center for Complementary and Integrative Health, National Institutes of Health, Bethesda, MD, USA

[2]Howard Hughes Medical Institute, Department of Neuroscience, Dorris Neuroscience Center, The Scripps Research Institute, La Jolla, CA, USA

***For correspondence: alexander.chesler@nih.gov**

Competing interest: The authors declare no that no competing interests exist.

ABSTRACT

Piezo1 is a stretch-gated ion channel required for mechanosensation in many organ systems. Recent provocative findings describe a new role for Piezo1 in the gut, suggesting that it is a sensor of microbial single-stranded RNA (ssRNA) rather than mechanical force. If true, this would redefine the scope of Piezo biology. Here, we sought to replicate the central finding that fecal ssRNA is a natural agonist of Piezo1. While we observed that fecal extracts and ssRNA stimulate calcium influx in certain cell lines, this response was independent of Piezo1. Additionally, sterilized dietary extracts devoid of gut biome RNA showed similar cell line-specific stimulatory activity to fecal extracts. Together, our data highlight potential confounds inherent to gut-derived extracts, exclude Piezo1 as a receptor for ssRNA in the gut, and support a dedicated role for Piezo channels in mechanosensing.

INTRODUCTION

Piezo proteins are mechanically gated ion channels that transduce changes in plasma membrane tension into electrical current (Ridone et al., 2019; Szczot et al., 2021). There are two members in the mammalian Piezo family: Piezo1 and Piezo2 (Coste et al., 2010). Piezo1 is expressed in many tissues including the cardiovascular, hematopoietic, and skeletal systems (Jiang et al., 2021; Li et al., 2014; Retailleau et al., 2015; Rode et al., 2017; Sun et al., 2019; Wang et al., 2016). Specifically, Piezo1 mediates the mechanical sensing of fluid flow and is required for normal development and function of lymph and blood vessels (Li et al., 2014; Liu et al., 2020; Nonomura et al., 2018; Ranade et al., 2014b). Additionally, many blood cell types depend on Piezo1 for shear force sensing and volume regulation (Cahalan et al., 2015; Cinar et al., 2015; Faucherre et al., 2014; Solis et al., 2019). These vascular functions are particularly evident in the clinical manifestation of Piezo1 mutations in humans (Albuisson et al., 2013; Bae et al., 2013; Fotiou et al., 2015; Glogowska et al., 2017; Lukacs et al., 2015). Piezo1 also regulates the formation and maintenance of bone and cartilage through mechanical load sensing (Hendrickx et al., 2021; Lee et al., 2014; Li et al., 2019; Sun et al., 2019; Wang et al., 2020; Zhou et al., 2020). In other organ systems, the role of Piezo1 is currently less well-defined, but it is known to function as a mechanosensor in neural stem cells and certain epithelial and mesenchymal cell types (Eisenhoffer et al., 2012; Martins et al., 2016; Miyamoto et al., 2014; Pathak et al., 2014; Sugimoto et al., 2017). By contrast, the homologous Piezo2 is expressed at its highest levels in the somatosensory system, vagal-nodose complex, and specialized epithelial cells (Chiu et

al., 2014; Kupari et al., 2019; Nguyen et al., 2017; Usoskin et al., 2015; Wang et al., 2017; Woo et al., 2014). Piezo2 is responsible for detecting gentle touch, vibration, and proprioception in mice and humans (Chesler et al., 2016; Ranade et al., 2014a; Woo et al., 2015).

Many extrinsic factors can influence Piezo mechanosensitivity including membrane tension, membrane voltage, cytoskeletal integrity, extracellular matrix contact, cyclic adenosine monophosphate signaling, and phosphatidylinositol second messenger pathways (Borbiro et al., 2015; Dubin et al., 2012; Gaub and Müller, 2017; Moroni et al., 2018; Narayanan et al., 2018; Romero et al., 2019, 2020). In addition to this list, it stands to reason that there could be ligands of Piezo channels that modulate or even directly evoke channel gating. Indeed, high-throughput drug screens have generated the synthetic small molecules called Yoda1, Jedi1, and Jedi2, which act as allosteric modulators of Piezo1 by stabilizing its open conformation (Botello-smith et al., 2019; Syeda et al., 2015; Wang et al., 2018).

Recently, a provocative study provided the first evidence of endogenous ligands for Piezo channels (Sugisawa et al., 2020). Remarkably, it was shown that Piezo1 in the mouse gut is not activated by mechanical forces but instead functions as a ligand-gated ion channel to sense single-stranded RNAs (ssRNAs). It was proposed that bioactive ssRNAs are produced by the gut microbiome, and that these molecules function through Piezo1 channels to alter serotonin production and trigger a physiological cascade that impacts bone homeostasis. Considering that ssRNAs might be generated and released under a variety of circumstances, the scientific field will have to radically rethink the role of Piezo1 not only in the gut but throughout the body. It also suggests

that perhaps Piezo2 can be gated by these types of molecules. Piezo2 is expressed by sensory and vagal neurons targeting the skin and other organ systems with diverse microbiomes that are also sites of viral infections and colonization by pathogenic bacteria or fungi (Chiu et al., 2014; Kupari et al., 2019; Nguyen et al., 2017; Usoskin et al., 2015; Wang et al., 2017; Woo et al., 2014). Therefore, we set out to use calcium imaging and electrophysiological recordings to investigate how ssRNAs derived from the gut influence Piezo channel function.

RESULTS

ssRNA40 does not alter calcium activity or mechanotransduction in N2a cells

ssRNA40 is a synthetic 20-mer ssRNA oligonucleotide derived from the human immunodeficiency virus (HIV) genome (Heil et al., 2004). ssRNA40 is classically known as an agonist for the immune surveillance toll-like receptor 7 and 8 in mice and humans, respectively (Heil et al., 2004; Zhang et al., 2018). However, it was recently reported that ssRNA40 also shows agonist activity toward the mechanosensitive ion channel Piezo1 (Sugisawa et al., 2020). To test this finding, we first used the Neuro-2a (N2a) mouse neuroblastoma cell line since these cells natively express Piezo1 (Coste et al., 2010) and were reported to conduct a Piezo1-dependent current in the presence of ssRNA40 (Sugisawa et al., 2020).

For measuring Piezo1 activity during exposure to ssRNA40, we performed *in vitro* fluorescent calcium imaging on N2a cell cultures with the Fluo-4 AM ester dye. Using ssRNA40 from the same supplier and dosage as prior studies (10 μg/mL) (Sugisawa et al., 2020), we found that application of ssRNA40 did not elicit a detectable increase in fluorescence, even when the imaging time frame was extended up to 3 minutes (Figure 1A and Video S1). As a positive control for Piezo1 activation, we used Yoda1, which is known to induced Piezo1-dependent calcium transients (Syeda et al., 2015). 30 μM Yoda1 triggered a dramatic calcium influx over the course of ~1 minute in virtually all N2a cells (Figures 1A – 1C). This was followed by application of ionomycin, a potent calcium ionophore, as a further positive control to elicit maximal calcium influx in all cells. For negative controls, we tested the vehicle solution alone to observe

mechanosensitive flow responses, and we tested ssRNA41 to examine sequence-specific effects of ssRNA (Figure 1A). ssRNA41 is the same length and sequence as ssRNA40, except all uridine residues are substituted with adenosine; unlike ssRNA40, this molecule is not a TLR7/8 agonist (Heil et al., 2004). After autofluorescence subtraction, there was no significant difference in N2a cell calcium activity between these negative controls and ssRNA40 (Figure 1C).

In addition to directly activating Piezo1, ssRNA40 was reported to delay the inactivation of Piezo1 mechanically evoked currents (Sugisawa et al., 2020), similar to Yoda1 (Syeda et al., 2015). We tested this claim by whole-cell voltage-clamp recordings of N2a cells during simultaneous mechanical stimulation of the plasma membrane. Mechanical stimuli were administered with a nanomotor probe to indent the cell surface in 1 μm increments (Video S2). The stimulation elicited a rapidly inactivating inward current, which is characteristic to the Piezo family of ion channels (Figure 1D). As expected, including 30 μM Yoda1 in the external bath solution resulted in a reduced apparent mechanical activation threshold and a prolonged inactivation phase of the currents (Figures 1D and 1E). By contrast, 10 μg/mL ssRNA40 in the bath solution showed no measurable change from the vehicle control on the amplitude, activation threshold, or inactivation rate of mechanically evoked currents (Figures 1D and 1E).

Figure 1

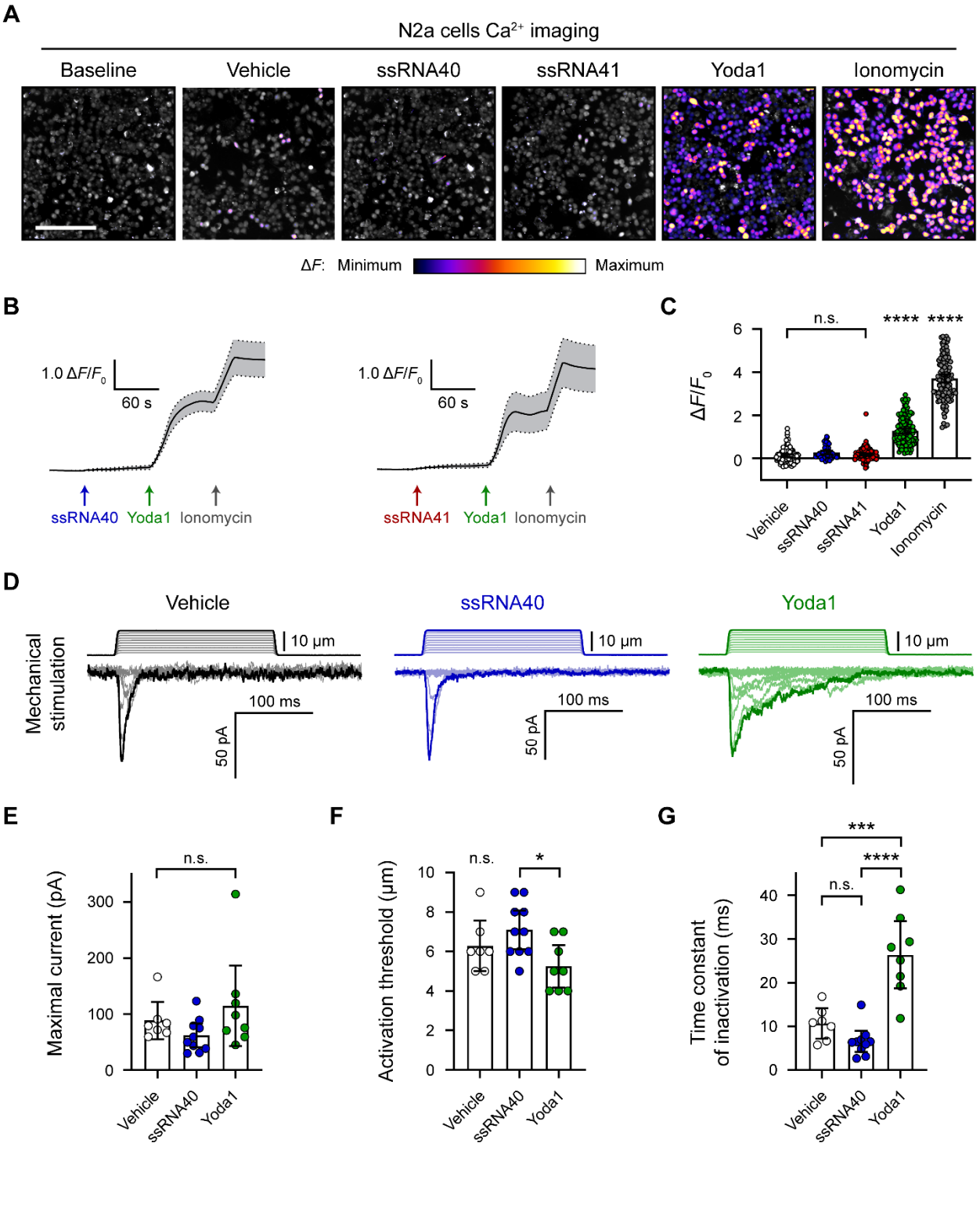

Figure 1

ssRNA40 does not alter calcium activity or mechanotransduction in N2a cells

(A) Fluo-4 calcium imaging of N2a cells during exposure to different treatments, representative of ≥ 3 independent recordings for each condition. The magnitude of the change in fluorescence (ΔF) is represented on a fire color scale and is superimposed on a grayscale baseline fluorescence image. Cells were exposed to buffer only (vehicle) or 10 µg/mL ssRNA40 or ssRNA41 for up to 3 minutes, followed by 30 µM Yoda1 and 10 µM ionomycin. Scale bar is 200 µm.

(B) Example calcium imaging traces of ssRNA40 and ssRNA41, each followed by Yoda1 and ionomycin control treatments. Only cells that responded to Yoda1 (functionally expressing Piezo1) were analyzed. Fluorescence values are shown as ΔF normalized to the initial fluorescence ($\Delta F/F_0$). n = 50 cells plotted as mean ± 95% confidence interval (CI).

(C) Quantification of calcium responses to different treatments. n = 50 cells per condition. Error bars indicate mean ± 95% CI. One-way ANOVA with Bonferroni correction: not significant (n.s.) $p \geq 0.05$, **** $p < 0.0001$.

(D) Example whole-cell voltage-clamp recordings of N2a cells during mechanical stimulation. Top traces indicate the magnitude of plasma membrane indentation in 1 µm steps, and bottom traces show whole-cell currents elicited by the stimuli. Vehicle, 10 µg/mL ssRNA40, or 30 µM Yoda1 were bath-applied 10 minutes prior to recording.

(E – G) Quantification of mechanically evoked current amplitude, threshold, and inactivation. n = 7 – 10 cells per condition. Error bars represent mean ± 95% CI. One-way ANOVA with Bonferroni correction: n.s. $p \geq 0.05$, * $p < 0.05$, *** $p < 0.001$, **** $p < 0.0001$.

ssRNA40 does not activate *Piezo1*-transfected HEK293 cells

Compared to the Piezo1 agonist activity of Yoda1, ssRNA40 was reported to have a relatively small effect size (Sugisawa et al., 2020). We were concerned that such a small effect size could have been overlooked in our initial experiments, given the relatively low functional expression of Piezo1 in N2a cells. Therefore, we also examined the effects of ssRNA on Piezo1 channels expressed at high levels via transient transfection of human embryonic kidney 293 (HEK293) cells. We performed calcium imaging to compare the responses of native versus *Piezo1*-transfected HEK293 cells during exposure to vehicle, ssRNA40, or ssRNA41 (Figures 2A and 2B). Each imaging trial was followed by stimulation with Yoda1 and ionomycin as positive controls for Piezo1 response and maximal response, respectively. There was a noticeable but nonsignificant calcium response of untransfected cells to Yoda1 (Figure 2C), consistent with a previous report that HEK293 cells express very low but detectable levels of human Piezo1 (Dubin et al., 2017). However, in both untransfected and *Piezo1*-transfected conditions, we found no significant calcium activity between vehicle, ssRNA40, and ssRNA41 (Figure 2C).

Prior studies used between 5 and 20 μg/mL ssRNA40 in their experiments (Heil et al., 2004; Lehmann et al., 2012; Shibata et al., 2016; Sugisawa et al., 2020). For that reason, our above experiments used 10 μg/mL ssRNA40. However, to explore whether ssRNA40 has a dose-response effect on Piezo1, we performed calcium imaging on *Piezo1*-transfected HEK293 cells during exposure to different concentrations of ssRNA40. Using a log scale range from 0.05 to 50 μg/mL, we did not observe significant calcium influx triggered by ssRNA40 at any concentration (Figure 2D).

Figure 2

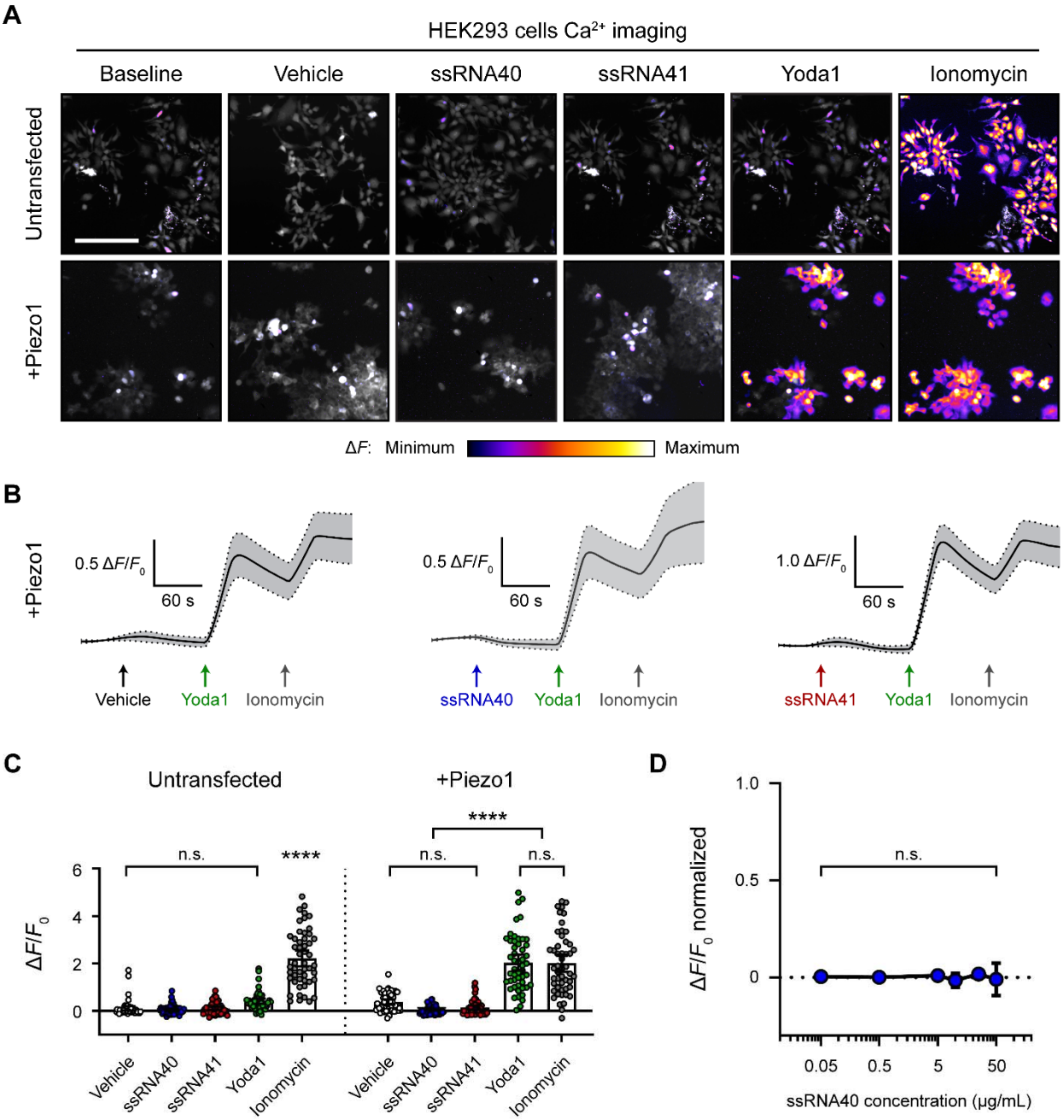

Figure 2

ssRNA40 does not activate *Piezo1*-transfected HEK293 cells

(A) Fluo-4 calcium imaging of HEK293 cells, with or without transfection of mouse *Piezo1*, representative of ≥ 3 independent recordings for each condition. Treatment concentrations are 10 μg/mL ssRNA40 or ssRNA41, 30 μM Yoda1, and 10 μM ionomycin. Scale bar is 200 μm.

(B) Example calcium imaging traces of *Piezo1*-transfected HEK293 cells during different treatments. Yoda1 was applied 90 seconds after any given RNA sample, and only cells that responded to Yoda1 (presumably Piezo1-transfected) were analyzed. Transfection efficiency was generally > 60% of the cell culture. n = 50 cells plotted as mean ± 95% CI.

(C) Quantification of HEK293 cell calcium responses. n = 50 cells per condition plotted as mean ± 95% CI. One-way ANOVA with Bonferroni correction: n.s. $p \geq 0.05$, **** $p < 0.0001$.

(D) Dose-response curve of ssRNA40 treatment on *Piezo1*-transfected GCaMP6s-expressing HEK293 cells. After 1 minute of baseline measurement, ssRNA40 was administered for 3 minutes followed by ionomycin for 1 minute. A random selection of cells was analyzed from each recording. The responses are normalized, with the ionomycin response being $\Delta F/F_0 = 1$. n = 25 cells per dose plotted as mean ± 95% CI. One-way ANOVA with Bonferroni correction: n.s. $p \geq 0.05$.

See also Figure S1.

An inability to replicate a finding could reflect unappreciated nuances in how two groups conduct the experiments. To address this possibility, we tested if ssRNA40 could activate Piezo1 in a completely independent laboratory using a distinct cell line, a different methodology, and separately sourced reagents. For these studies, we used a Piezo1-knockout (Piezo1-KO) genetic background HEK293 cell line (Dubin et al., 2017). Importantly, this is the identical cell line used in the originally published ssRNA experiments on Piezo1 (Sugisawa et al., 2020). We recorded the calcium response to ssRNA40 with or without *Piezo1* transfection using a fluorescence imaging plate reader (FLIPR) calcium flux screening platform. Several ssRNA40 concentrations were tested from 0.312 to 5 μg/mL followed by Yoda1 as a positive control. We compared untransfected cells to cells transfected with either mouse *Piezo1* or human *Piezo1* (Figure S1A. No increase in calcium was detected throughout exposure to ssRNA40, and there were no significant differences between transfected and untransfected cells or across the various ssRNA40 concentrations (Figure S2A). To examine if ssRNA40 might more subtly potentiate Piezo1 activity, we checked whether the response to 5 μM Yoda1 was increased after exposure to ssRNA40. However, we found no change in the Yoda1 response following treatment with vehicle or different ssRNA40 concentrations (Figure S2A). Together, these data independently corroborate our previous observations that ssRNA40 does not activate Piezo1 directly or modulate its mechanotransduction in either N2a cells or HEK293 cells.

Figure S1

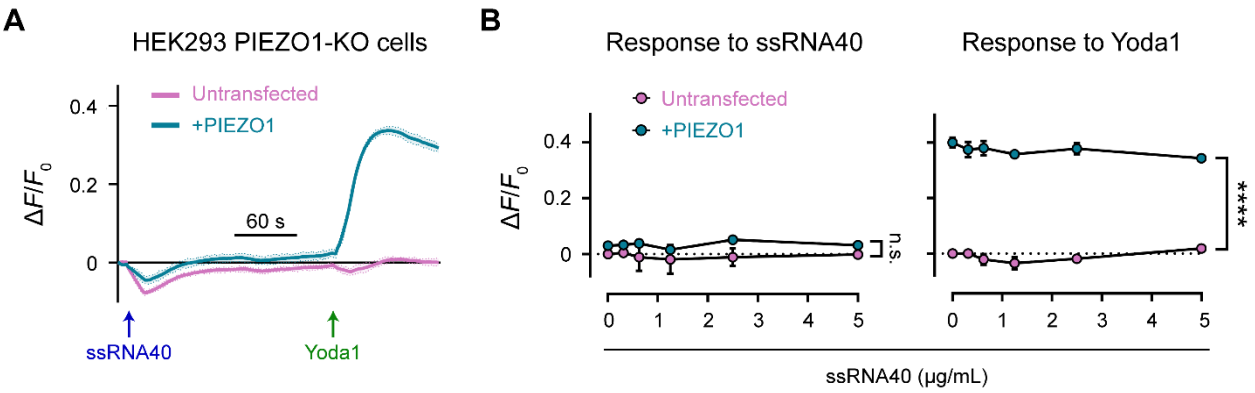

Figure S1, related to Figure 2

ssRNA40 does not activate Piezo1 or modify its response to Yoda1

(A) FLIPR assay on HEK293 Piezo1-KO cells, with or without transfection of human *Piezo1*. Treatment concentrations are 5 µg/mL ssRNA40 and 5 µM Yoda1. n = 4 wells per condition plotted as mean ± standard error of the mean (SEM).

(B) Quantification of FLIPR calcium recordings of ssRNA40 dose-response and its effect on Yoda1 response. n = 4 wells per condition plotted as mean ± SEM. Pairwise comparisons between untransfected and transfected recordings using multiple unpaired t-tests with 5% false discovery rate: n.s. $q \geq 0.05$, **** $q < 0.0001$.

Fecal and dietary extracts activate HEK293 cells independently of Piezo1

The concept that ssRNA can activate Piezo1 originally arose from screening components of mouse feces and led to the hypothesis that compounds produced by the gut microbiome directly influence Piezo1 function. It was reported that both crude fecal extracts and purified fecal RNA elicit a calcium influx in *Piezo1*-transfected HEK293 cells (Sugisawa et al., 2020). Although the synthetic ssRNA40 molecule did not activate Piezo1 in our hands, it remained possible that fecal preparations could show agonist activity. We homogenized and diluted mouse fecal matter to 100 mg/mL and filtered it through a 0.45 μm mesh to eliminate any undissolved sample. Pipetting this solution onto cells resulted in extremely high autofluorescence that precluded calcium imaging. However, we found that the autofluorescence was mostly eliminated if the feces were diluted to at least 5 mg/mL – we refer to this diluted filtered sample as “fecal extract”. Applying fecal extract to *Piezo1*-transfected HEK293 cells triggered a substantial calcium response (Figure 3A and Video S3). More dilute preparations of extract yielded little or no calcium influx. Interestingly, across several imaging trials, we noticed that the response to 5 mg/mL fecal extract was variable; not all cells in the field of view would necessarily respond, and the response onset was often 30 – 60 seconds after the fecal extract was first added (Figures 3A and 3B). Notably, however, we also found that untransfected HEK293 cells had a similar calcium response to fecal extract, suggesting that fecal extracts may trigger calcium influx via a Piezo1-independent mechanism (Figures 3A and 3B). This was confirmed by applying fecal extract to Piezo1-KO HEK293 cells, which still responded despite the complete absence of Piezo1 (Figures S2A and S2B).

Crude fecal extracts are complex biochemical mixtures that include products from the microbiome. To test the contribution of bacterial RNA in the calcium response of HEK293 cells to fecal extract, we purified these nucleic acids (Figure 3C) from our samples and tested if they activated Piezo1. In contrast to the total extract, we did not observe a detectable calcium influx with 10 μg/mL fecal RNA – the same concentration used in other studies (Figure 3D) (Sugisawa et al., 2020). We additionally extracted fecal RNA using the same kit and procedure as prior studies (Sugisawa et al., 2020), but this sample likewise failed to induce any activity (see Materials and Methods). We then performed the reciprocal experiment by treating fecal extracts with the ssRNA-degrading enzyme RNase A. Both RNase-treated and untreated fecal extracts activated *Piezo1*-transfected HEK293 cells to a similar degree (Figure 3D). Together, these experiments demonstrate that fecal extracts can stimulate calcium influx in HEK293 cells, but this effect is unlikely to be mediated by RNA and, regardless, the activity does not depend on Piezo1.

To disentangle possible sources of activation in our fecal extracts, we evaluated whether anything in the mouse diet might stimulate HEK293 cell calcium influx. We reasoned that separately testing the food input would eliminate host and microbial factors found in the fecal output. Mouse chow pellets were dissolved and filtered to prepare a dietary extract by the same method as the previous fecal extracts. Surprisingly, applying 5 mg/mL dietary extract to HEK293 cells produced a substantial calcium response (Figure 3E). This activation occurred in both untransfected and *Piezo1*-transfected cells. Similar to fecal extract, the dietary extract often activated only a subset of cells (Figure 3E and Video S4). The timing of the response onset was also

variable but tended to occur earlier compared to fecal extract (Figure 3F). Dietary extract also activated Piezo1-KO HEK293 cells, confirming that Piezo1 is dispensable for the response to the extract (Figures S2A and S2B). To verify that the dietary and fecal extracts were not activating cells in a nonspecific way by changing the osmolality or pH, we confirmed that these properties were not substantially altered between control solutions and the crude extracts (see Materials and Methods). These results suggest that an element of the mouse diet, if present in fecal matter, could be a confounding factor when studying active compounds derived from the host gut or resident microbiota in calcium imaging assays.

Figure 3

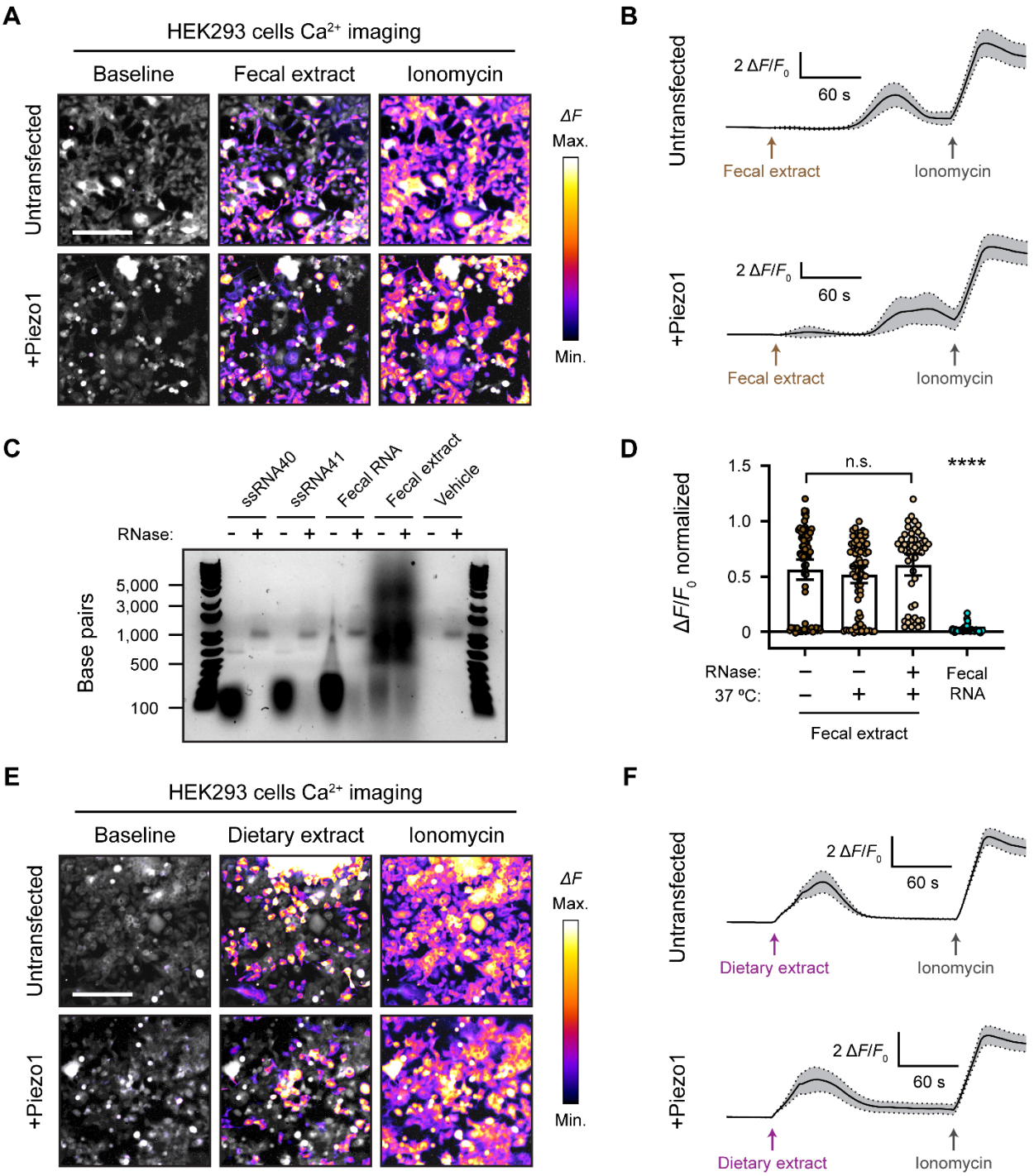

279

Figure 3

Fecal and dietary extracts activate HEK293 cells independently of Piezo1

(A) GCaMP6s calcium imaging of HEK293 cells during exposure to 5 mg/mL fecal extract, with or without *Piezo1* transfection, representative of ≥ 3 independent recordings for each condition. Scale bar is 200 μm.

(B) Example calcium imaging traces of HEK293 cell responses to fecal extract. n = 50 cells per condition plotted as mean ± 95% CI.

(C) Agarose gel showing the nucleic acid content of 50 μg/mL purified fecal RNA and 100 mg/mL crude fecal extract. 50 μg/mL of ssRNA40 and ssRNA41 were used as positive controls since they are pure RNA samples of a defined mass and sequence. Ringer's solution was used as vehicle negative control. Treating the samples with RNase A eliminated the low molecular weight nucleic acid (< 500 bp). The crude fecal extract additionally had a high molecular weight smear (500 – 5,000 bp) that was unaffected by RNase A treatment, which is likely DNA.

(D) Quantification of *Piezo1*-transfected HEK293 cell responses to 5 mg/mL fecal extracts that were untreated (control), heat-treated (mock), or heat + RNase A-treated (RNase), as well as 10 μg/mL fecal RNA. The $\Delta F/F_0$ values are normalized, with the ionomycin response being $\Delta F/F_0$ = 1. n = 50 cells per condition plotted as mean ± 95% CI. Kruskal-Wallis with Dunn's multiple comparisons test: n.s. $p \geq 0.05$, **** $p < 0.0001$.

(E) GCaMP6s calcium imaging of HEK293 cells during exposure to 5 mg/mL dietary extract, with or without *Piezo1* transfection, representative of ≥ 2 independent recordings for each condition Scale bar is 200 μm.

(F) Example calcium imaging traces of HEK293 cell responses to dietary extract. n = 50 cells per condition plotted as mean ± 95% CI.

See also Figure S2.

Figure S2

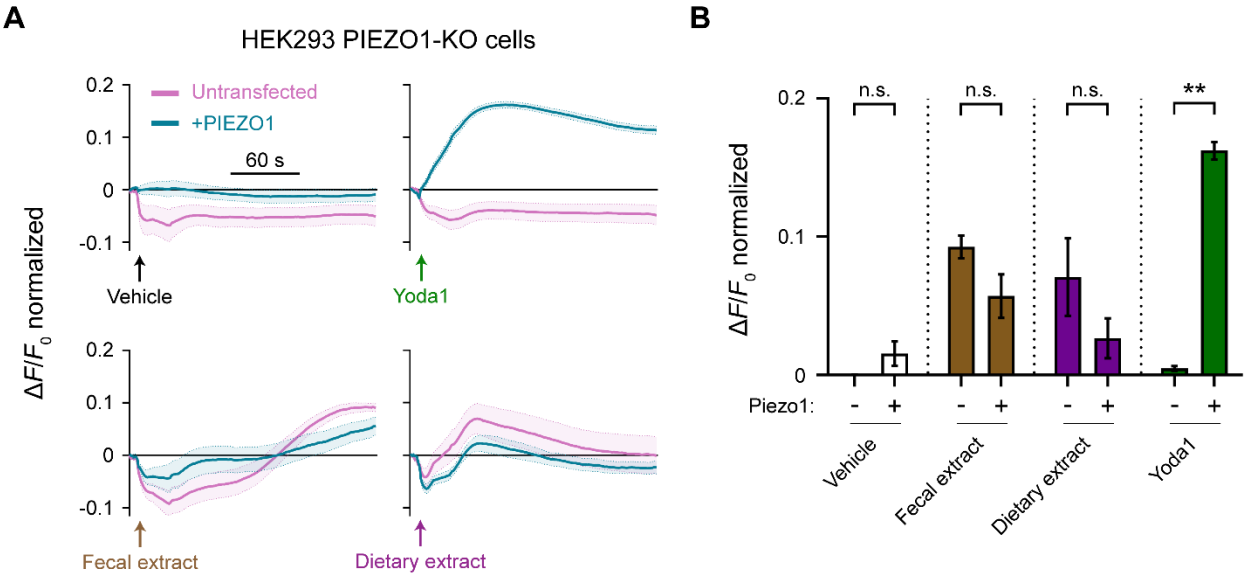

Figure S2, related to Figure 3

Fecal and dietary extracts activate HEK293 Piezo1-KO cells

(A) FLIPR assays on HEK293 Piezo1-KO cells, with or without transfection of human *Piezo1*. Each treatment condition was followed up with ionomycin to elicit maximum response for normalization (not shown). Treatment concentrations are 5 mg/mL fecal or dietary extract, 5 μM Yoda1, and 10 μM ionomycin. n = 4 wells per condition plotted as mean ± SEM.

(B) Quantification of FLIPR calcium recordings for different treatments. n = 4 wells per condition plotted as mean ± SEM. Kruskal-Wallis with Dunn's multiple comparisons test: n.s. $p \geq 0.05$, ** $p < 0.01$.

317 Piezo1 is a non-selective ion channel that inactivates quickly (within 10 – 30 ms)
318 (Coste et al., 2010). Therefore, calcium imaging is not the most sensitive readout of
319 channel gating. To more definitively confirm that fecal extracts and ssRNA are not
320 affecting Piezo1 activity, we carried out a series of whole-cell voltage-clamp recordings
321 on *Piezo1*-transfected HEK293 cells. The cells were mechanically stimulated in the
322 presence of ssRNA40 or fecal extract (Figure 4A). As negative and positive controls for
323 Piezo1 agonism, vehicle solution and Yoda1 were used respectively. Across all
324 conditions, the maximum whole-cell Piezo1 current evoked by mechanical stimulation
325 was unchanged (Figure 4B). By contrast, Yoda1 significantly lowered the apparent
326 mechanical threshold for Piezo1 activation (Figure 4C) and delayed channel inactivation
327 (Figure 4D), as expected (Syeda et al., 2015). Together, our results do not provide
328 evidence for even a limited effect of either ssRNA40 or fecal extracts on the biophysical
329 properties of Piezo1 (Figures 4B – 4D).
330

Figure 4

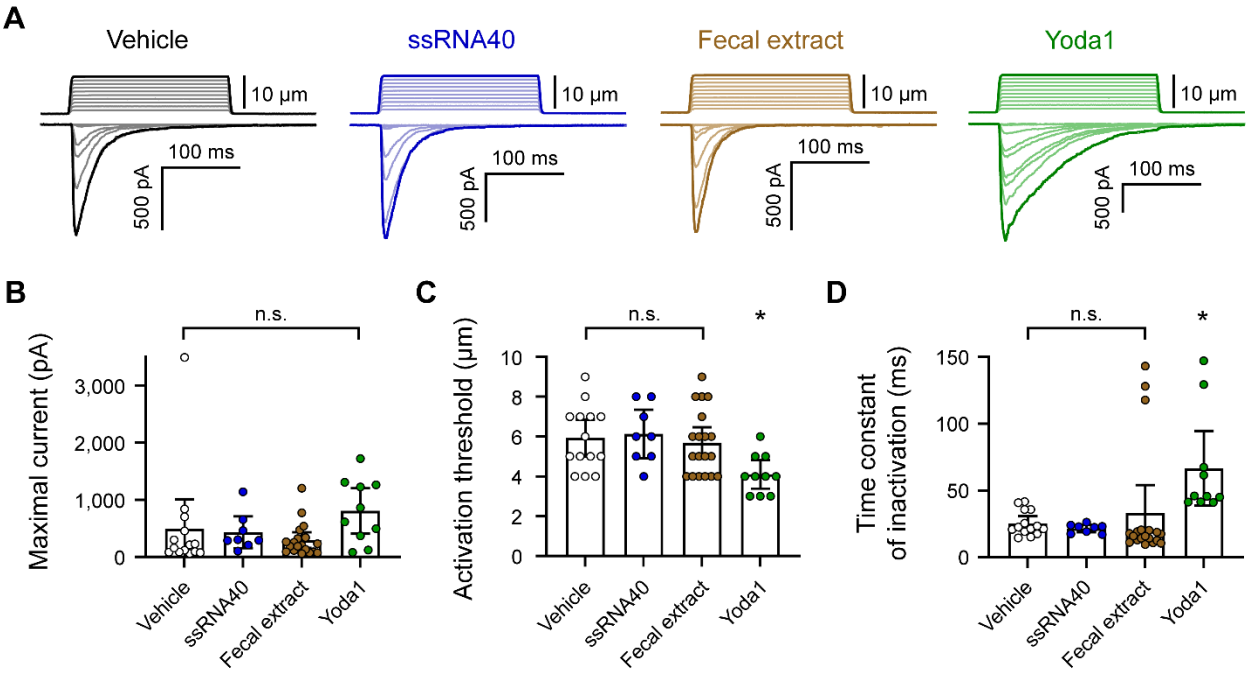

Figure 4

ssRNA40 and fecal extract do not modify Piezo1 mechanotransduction

(A) Example whole-cell voltage-clamp recordings of *Piezo1*-transfected HEK293 cells during mechanical stimulation. Top traces indicate the magnitude of plasma membrane indentation in 1 µm steps, and bottom traces show whole-cell currents elicited by the stimuli. Vehicle, 10 µg/mL ssRNA40, 5 mg/mL fecal extract, or 30 µM Yoda1 were bath-applied 5 minutes prior to recording.

(B – D) Quantification of mechanically evoked current amplitude, threshold, and inactivation. Individual cell responses are plotted: n = 14 vehicle, n = 8 ssRNA40, n = 19 fecal extract, and n = 10 Yoda1. Error bars represent mean ± 95% CI. One-way ANOVA with Bonferroni correction: n.s. $p \geq 0.05$, * $p < 0.05$.

343 **Calcium response to fecal and dietary extracts is cell line-specific**

344 We were concerned about the potential confounding effect of fecal/dietary
345 extract-induced activation of HEK293 cells, and we wondered whether this effect
346 extended to other commonly used cell lines in the field. Piezo1 was originally
347 discovered in N2a cells (Coste et al., 2010), and this cell line continues to be frequently
348 used for *in vitro* work on Piezo1 (Geng et al., 2020; Ridone et al., 2020; Romero et al.,
349 2019). Therefore, we compared N2a and HEK293 cells, with or without *Piezo1*
350 transfection, during treatment with fecal/dietary extracts. Since Piezo1 is endogenously
351 expressed in wildtype N2a cells, we performed these experiments on a Piezo1-knockout
352 (Piezo1-KO) N2a cell line (Moroni et al., 2018).

353 The untransfected N2a Piezo1-KO cells showed no calcium response to Yoda1
354 treatment, confirming an absence of Piezo1 (Figure 5A). Conversely, N2a Piezo1-KO
355 cells that were transfected with *Piezo1* showed a large calcium response to Yoda1,
356 confirming an efficient transfection. Interestingly, unlike HEK293 cells, N2a cells did not
357 respond to either fecal or dietary extracts (Figure 5A). Moreover, *Piezo1* transfection did
358 not endow N2a cells with sensitivity to either of these extracts (Figure 5B). From these
359 data, we conclude that neither fecal extracts nor RNA derived from the gut microbiome
360 can activate Piezo1. Instead, fecal/dietary extract sensitivity appears to be linked to
361 other cell line-specific factors found in HEK293 cells but not N2a cells.

362

363

Figure 5

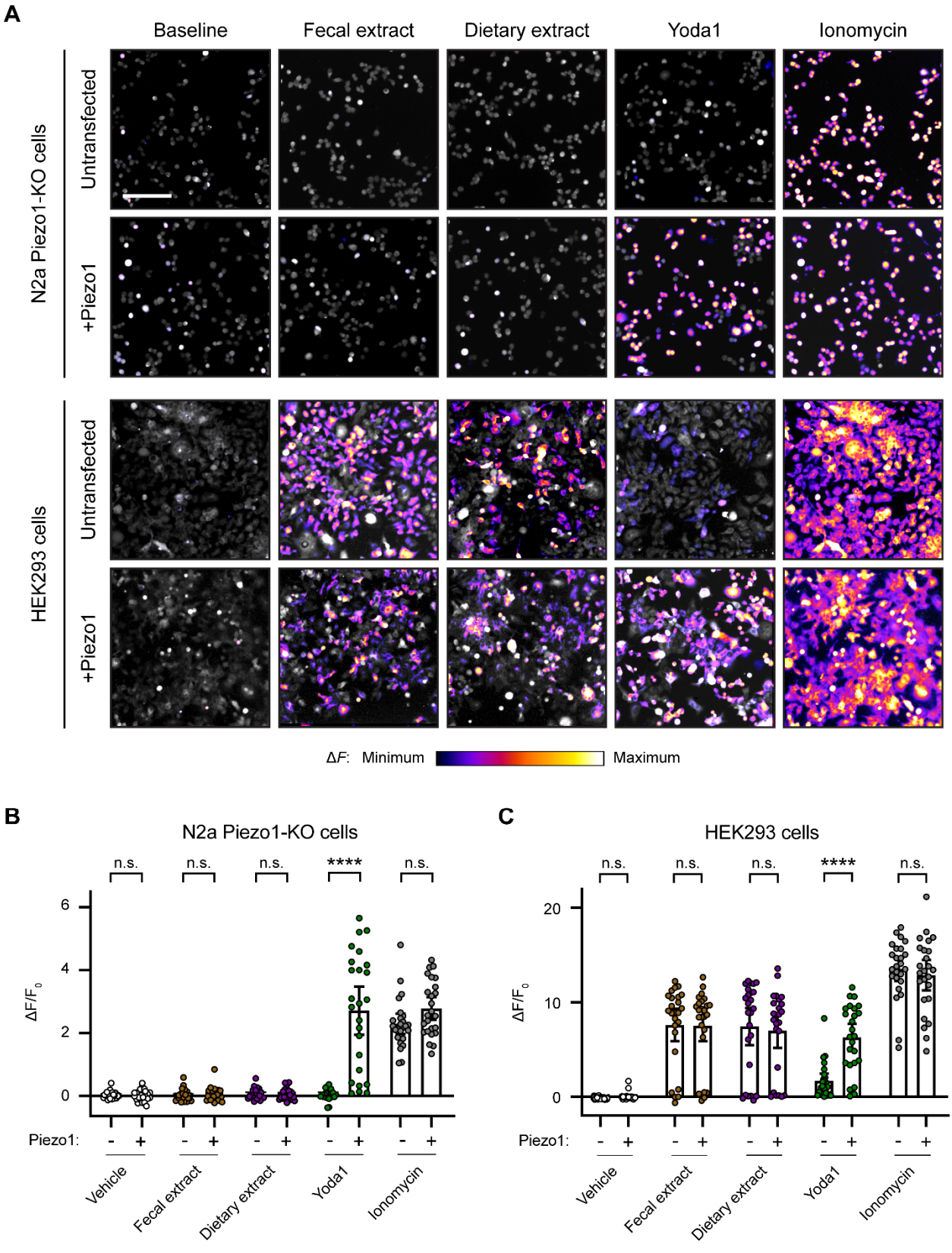

364

Figure 5

Fecal and dietary extracts induce cell line-specific activity independently of Piezo1

(A) Calcium imaging of N2a Piezo1-KO cells and HEK293 cells, with or without *Piezo1* transfection, representative of ≥ 2 independent recordings for each condition. Fluo-4 or GCaMP6s were used to image the N2a cells or HEK293 cells, respectively. Treatment concentrations are 5 mg/mL fecal or dietary extract, 30 μM Yoda1, or 10 μM ionomycin. Scale bar is 200 μm.

(B) Quantification of calcium responses. n = 25 cells per condition plotted as mean ± 95% CI. Pairwise comparisons between untransfected and transfected recordings using Kruskal-Wallis with Dunn's multiple comparisons test: n.s. $p \geq 0.05$, **** $p < 0.0001$.

RNA activates RIN14B cells independently of Piezo1

Considering that RNA-sensing by Piezo1 was originally investigated in the gut (Sugisawa et al., 2020), we sought to continue our exploration of the effect of ssRNAs in a physiologically relevant cell line, RIN14B. This pancreatic endocrine cell line is commonly used to model gut enterochromaffin cell function and natively expresses Piezo1 (Nozawa et al., 2009; Sugisawa et al., 2020). To examine the effect of ssRNAs on these cells, we performed calcium imaging in RIN14B cells transfected with GCaMP6s. We measured the change in fluorescence following addition of vehicle, ssRNA40, ssRNA41, fecal RNA, or Yoda1. Each imaging trial was followed by application of ionomycin to determine maximal fluorescence. As expected from previous experiments, the vehicle caused no significant change (Figures 6A – C). However, ssRNA40 and ssRNA41 elicited a noticeable calcium response in RIN14B cells, unlike in N2a or HEK293 cells (Figure S3A). Fecal RNA also elicited a calcium response, similar in magnitude to that caused by ssRNA40 and ssRNA41 (Figures 6D – F and Video S5). In comparison, Yoda1 led to a significantly larger increase in fluorescence, consistent with endogenous expression of Piezo1 in RIN14B cells (Figures 6G – I).

To investigate the dependency between the RNA-evoked response and Piezo1 function in these cells, we performed calcium imaging on RIN14B cells in the presence of gadolinium. Gadolinium is a broad inhibitor of stretch-activated cation channels including Piezo1 (Coste et al., 2010). Cells were exposed first to gadolinium and then to either vehicle, fecal RNA, or Yoda1. At baseline, we noticed general effects of gadolinium on the excitability of RIN14B cells, evident by reduced spontaneous calcium transients during vehicle application (Figures 6B and 6C). Notably, gadolinium did not

diminish the response to fecal RNA, but it seemed to have a nonspecific effect on the decay rate of the calcium signal (Figures 6E and 6F). Gadolinium completely abolished the Yoda1 response, confirming successful Piezo1 inhibition (Figures 6H and 6I). Together, these experiments demonstrate that while RIN14B cells do respond to a variety of ssRNAs, their response is not dependent on Piezo1.

In addition to Piezo1, RIN14B cells and gut enterochromaffin cells express the electrophile receptor Trpa1 (Bellono et al., 2017; Nozawa et al., 2009). We speculated that Trpa1 may be responsible for the RNA-induced calcium response, considering Trpa1 has been reported to respond to extracellular microRNAs (Park et al., 2014). To test this, we performed calcium imaging on RIN14B cells in the presence of a Trpa1 inhibitor, A-967079. As expected, the Trpa1 inhibitor blocked the calcium response following addition of allyl isothiocyanate (AITC), an electrophilic Trpa1 agonist (Figure S3B). However, the Trpa1 inhibitor did not significantly diminish the calcium response following addition of ssRNA40 or ssRNA41 (Figure S3B), indicating that the RNA-induced response is not dependent on Trpa1.

To facilitate a better understanding of the molecular basis for extracellular ssRNA-sensing, we performed single-nuclei RNA sequencing on RIN14B cells. Algorithmic clustering of individual nuclear transcriptomes revealed a homogenous cell culture population without any meaningful transcriptomic sub-populations. As a starting point for identifying candidate ssRNA receptors, we compiled a gene list based on gene ontology annotations for ion channels, cation transmembrane transporters, and G protein-coupled receptors (Table 1). The rough expression prevalence of each gene is conveyed as the fraction of cells in which that gene's transcripts were detected.

Additionally, we have included the entire sequencing dataset as an open resource for investigating RIN14B cell gene expression (Table S1). We anticipate these data will be useful for more deeply assessing the fidelity of the RIN14B line as a model of gut enterochromaffin cells.

Figure 6

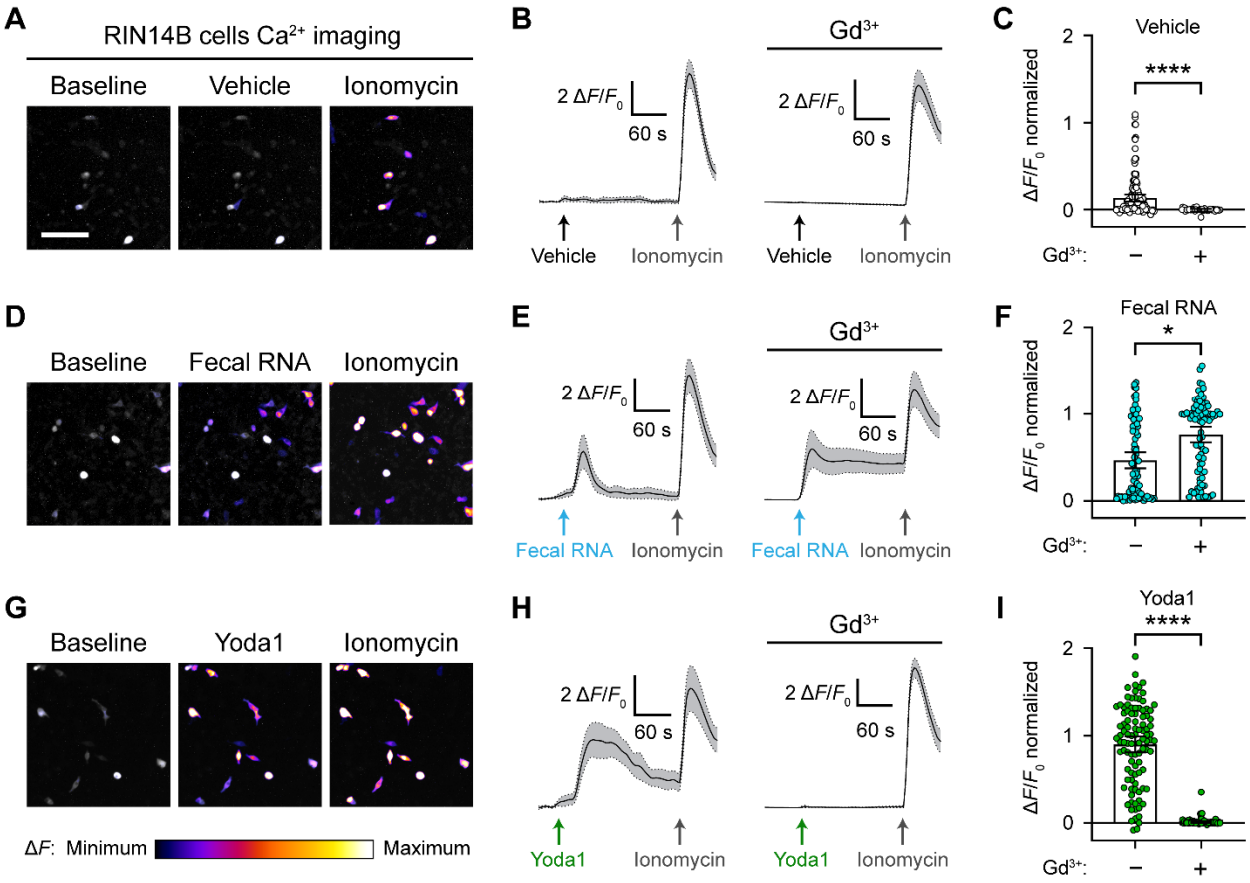

Figure 6

RNA activates RIN14B cells independently of Piezo1

(A – C) Calcium imaging of RIN14B cell activity during application of negative control vehicle with and without gadolinium inhibition of Piezo1. Gadolinium visibly reduced spontaneous calcium transients.

(D – F) RIN14B cell calcium influx in response to fecal RNA, with and without gadolinium.

(G – I) RIN14B cell calcium influx in response to the positive control Piezo1 agonist Yoda1, which is blocked by gadolinium. The calcium imaging was performed on GCaMP6s-transfected cells. GCaMP6s calcium responses were measured during stimulation with 25 μg/mL fecal RNA, 15 μM Yoda1, and 10 μM ionomycin. To block Piezo1, 30 μM gadolinium was pre-incubated on the cells for 5 minutes and included throughout the calcium imaging recording. Line graphs represent mean ± 95% CI of a single recording each of n = 50 cells. Bar graphs represent n = 100 – 150 cells from ≥ 2 independent recordings for each condition, with fluorescence values normalized to the response to ionomycin = 1.0, and the bars indicate mean ± 95% CI. Pairwise comparisons between untreated and gadolinium (Gd3+)-treated recordings using Kruskal-Wallis with Dunn's multiple comparisons test: * $p < 0.05$, **** $p < 0.0001$. The scale bar for the microscope images is 100 μm.

Figure S3

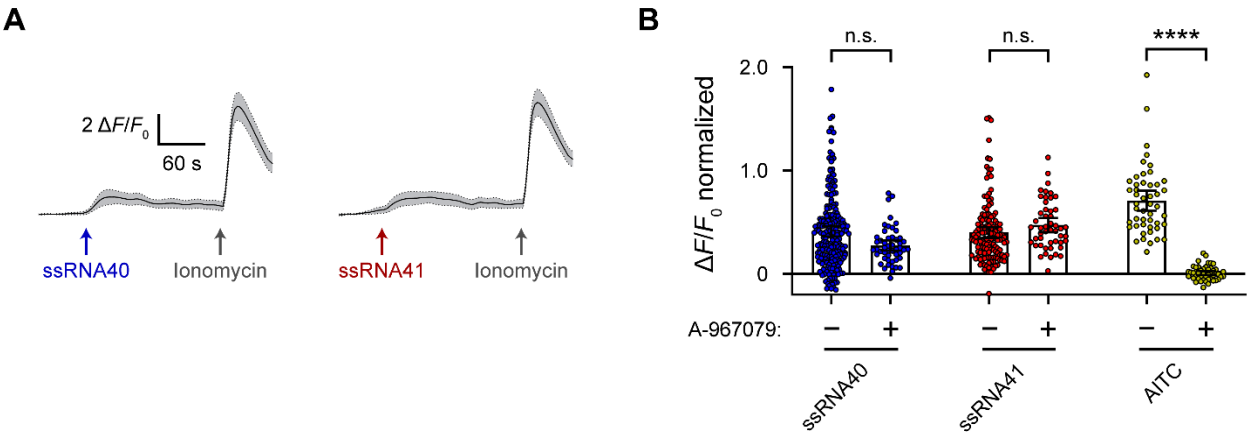

Figure S3

RNA activates RIN14B cells independently of Trpa1

(A) Calcium imaging of ssRNA40 and ssRNA41 responses in RIN14B cells loaded with Fluo-4 AM, representative of ≥ 3 independent recordings for each condition. Cells were stimulated with 25 µg/mL ssRNA40 or ssRNA41 and 10 µM ionomycin. The mean $\Delta F/F_0$ ± 95% CI is shown for a single recording each of n = 50 cells.

(B) To block Trpa1, 10 µM A-967079 was pre-incubated on the cells for 5 minutes and included throughout the calcium imaging recording. 10 µM AITC was used as a positive control for Trpa1 activation. Bar graphs represent n = 50 – 200 cells from 1 – 4 independent recordings for each condition, with fluorescence values normalized to the response to ionomycin = 1.0, and the bars indicate mean ± 95% CI. Pairwise comparisons between untreated and A-967079-treated recordings using Kruskal-Wallis with Dunn's multiple comparisons test: n.s. $p \geq 0.05$, **** $p < 0.0001$.

Table 1. Ion channels and GPCRs in RIN14B cells

"Ion channel activity" genes	Percent of cells expressing gene
Asic1	19.5
Asic2	42.7
Chrna7	7.7
Clcn3	42.1
Gabrb3	16
Kcnd3	13.5
Kcnh2	8.6
Kcnk3	12.3
Mcub	37.5
Tmem120a	16.3
Trpa1	15.2

"Cation transmembrane transport" genes	Percent of cells expressing gene
Ano10	10.6
Atp13a1	18.6
Atp13a3	30.7
Atp1b1	17.2
Cnga1	8.9
Grina	10.6
Mcoln1	16.9
Nalcn	9.5
Pex5l	63
Piezo1	9.2
Slc29a4	9.2
Slc30a7	38.4
Slc30a9	71.1
Slc41a2	16.6
Tmem63a	13.2
Tmem63b	35.5
Tmem63c	36.4
Tomm40	11.2
Trpm3	49.3
Trpm7	65.9
Unc80	41.3

"GPCR activity" genes	Percent of cells expressing gene
Adgra2	7.7
Adgra3	8
Adgrb2	9.2
Adgrb3	51
Adgrg1	16.9
Adgrg4	15.8
Adgrl1	22.1
Adgrl2	37.2
Adgrl3	61.3
Adgrv1	9.2
Celsr2	9.2
Celsr3	10.9
Glp1r	56.4
Gpr146	10.9
Gpr158	53.6
Gpr176	9.7
Gpr6	28.7
Gprc5b	14.3
Gprc5c	19.8
Grm1	23.5
Lgr4	19.8
Lpar6	9.7
Oxtr	8
Tas1r2	20.6
Tm2d1	22.9
Tpra1	9.2
Vom2r44	9.5

455

DISCUSSION

In this study, we set out to confirm the discovery that Piezo1 is a sensor of fecal microbiome ssRNA. We were not able to detect ssRNA-evoked changes in Piezo1 activity with *in vitro* calcium imaging and electrophysiological recordings. Instead, we present evidence that ssRNAs and fecal extracts can stimulate calcium influx in cultured cells, but this calcium activity depends on the cell line being used, rather than Piezo1 function. An unexpected finding is that dietary extracts can elicit calcium influx similar to fecal extracts. We also observed differential effects of fecal/dietary extracts between mouse colonies in different facilities, with some preparations showing more or less activity. This highlights the importance of controlling for elements of the diet when working with gut-derived samples.

Our data leave open questions regarding the sources of Piezo1 activation and possible functional roles for ssRNAs in the gut. Interestingly, our observation that the enterochromaffin model cell line RIN14B responds to ssRNAs corroborates the recent evidence that there exists a gut-resident RNA receptor (Sugisawa et al., 2020). However, we are unable to reproduce the finding that Piezo1 is an RNA receptor, and we propose that Piezo1 is more likely functioning as a mechanosensor in the gut, as has been shown in many other tissues (Murthy et al., 2017; Syeda, 2021; Zhao et al., 2019).

Supplemental figure legends

Figure 3-source data 1

Original uncropped RNA gel

RNA and fecal samples, untreated or RNase-treated, separated on a 1% agarose gel to examine the RNA content and effect of RNase on the samples.

Video S1

N2a cells do not respond to ssRNA40

5 minute time-lapse recording of fluo-4 AM fluorescence in N2a cells during sequential exposure to 10 μg/mL ssRNA40, 30 μM Yoda1, and 10 μM ionomycin. 1 second of video is equivalent to 30 seconds of real time.

Video S2

Mechanical stimulation assay

A HEK293 cell during simultaneous mechanical stimulation and whole-cell current recording. The patch pipette (left) is sealed onto the plasma membrane, and the mechanical probe (right) indents the cell membrane to evoke Piezo1 activity. The video depicts a single 5 μm indentation as part of a larger train of step-wise indentations from 1 to 10 μm.

Video S3

HEK293 cells respond to fecal extract

5 minute time-lapse of GCaMP6s fluorescence in HEK293 cells during exposure to 5 mg/mL fecal extract and then 10 μM ionomycin. 1 second of video is equivalent to 30 seconds of real time.

Video S4

HEK293 cells respond to dietary extract

5 minute time-lapse of GCaMP6s fluorescence in HEK293 cells during exposure to 5 mg/mL dietary extract and then 10 μM ionomycin. 1 second of video is equivalent to 30 seconds of real time.

Video S5

RIN14B cells respond to fecal RNA

5 minute time-lapse of GCaMP6s fluorescence in RIN14B cells during exposure to 25 μg/mL fecal RNA and then 10 μM ionomycin. 1 second of video is equivalent to 30 seconds of real time.

Acknowledgements

We thank Gary Lewin for generously providing the Piezo1-KO N2a cell line and the Janelia GENIE Project for the GCaMP6s sequence. Nick Ryba and Minh Nguyen performed the sample preparation and analysis of the single-nuclei RNA sequencing of RIN14B cells. We are grateful to Shang Ma, Chuan Wu, Jialie Luo, and Aisha AlJanahi for technical assistance in the study.

Funding

The research was funded by the National Center for Complementary and Integrative Health (NCCIH) and National Institute of Neurological Disorders and Stroke (NINDS) Intramural Research Programs (A.T.C.); the Howard Hughes Medical Institute and NIH R35 NS105067 (A.P.); and the National Center for Advancing Translational Sciences (NCATS) through the National Institutes of Health (NIH) Helping to End Addiction Long-term^{SM} (HEAL) Initiative. The content is solely the responsibility of the authors and does not necessarily represent the official views of the NIH or its HEAL initiative.

Author contributions

A.R.N., A.P., and A.T.C. conceived and designed the study. A.R.N., S.S., G.S.O., Y.Z., and M.N. performed all experiments. A.R.N., S.S., and G.S.O. analyzed the data and prepared figures. A.R.N. and G.S.O. wrote the initial draft of the manuscript. All authors edited the manuscript.

MATERIALS AND METHODS

Mice

All experiments involving mice adhered to the animal usage guidelines set by the National Institutes of Health (NIH) and were first approved by the National Institute of Neurological Disorders and Stroke (NINDS) Animal Care and Use Committee. Equal numbers of male/female wildtype C57BL/6J mice between the ages of 6 weeks and 1 year old were used. The mice were housed in an AAALAC International accredited pathogen-free facility with *ad libitum* access to food and water. Water was purified by reverse osmosis and then UV treated and chlorinated at 15 – 18 ppm such that after two weeks the chlorine concentration was ≥ 2 ppm. The diet consisted purely of the chemically defined Prolab® RMH 1800 (LabDiet, 5LL2) autoclaved rodent chow.

Cell culture

The following cell lines were used in the study: wildtype N2a cells (ATCC, CCL-131), Piezo1-KO N2a cells (Moroni et al., 2018), wildtype HEK293 cells (ATCC, CRL-1573), PIEZO1-KO HEK293 cells (Dubin et al., 2017), GCaMP6s HEK293 cells (this study), and RIN14B cells (ATCC, CRL-2059) (Nozawa et al., 2009). All cell lines were maintained on polystyrene culture plates (Fisher Scientific, 07-200-80) in a 5% CO_2 humidified incubator at 37 ºC. The growth medium was changed every 2 – 3 days and consisted of RPMI-1640 (for the RIN14B cells) (Fisher Scientific, 11-875-093) or otherwise DMEM/F12 (Fisher Scientific, 11330032) supplemented with 10% fetal bovine serum (Fisher Scientific, 26140079). Cells were passaged when they reached

561 confluence, which was roughly twice per week, and all cultures that were used for
562 experiments were not propagated beyond 20 passages. For passaging, cells were
563 rinsed in PBS (Fisher Scientific, 10010023) and then incubated in Accutase (Fisher
564 Scientific, 00-4555-56) for ~5 minutes at 37 ºC to detach. Cells were collected in a 15
565 mL tube (Fisher Scientific, 12-565-268) and centrifuged at 300 rcf for 3 minutes to
566 pellet. The supernatant was aspirated, and cells were resuspended in growth medium
567 followed by plating in new polystyrene plates. Typical dilution ratios for passaging were
568 between 1:3 and 1:20.
569

570 **Generating GCaMP6s stable HEK293 cells**

571 GCaMP6s was generated by a custom gene synthesis service (Epoch Life Science) and
572 subcloned into a pLV-CMV-PGK-Hyg lentiviral vector (Cellomics Technology, LVR-
573 1046) to make pLV-CMV-GCaMP6s-PGK-Hyg. This vector was used to produce
574 lentiviral particles (Vigene Biosciences). Then, wildtype HEK293 cells (ATCC, CRL-
575 1573) were infected in regular growth medium with 5 µg/mL polybrene (Sigma-Aldrich,
576 TR-1003-G) and the lentivirus at a multiplicity of infection of 5 viral particles per cell.
577 Transduction was allowed to occur overnight. The cells were then replated, and 48
578 hours later 100 µg/mL Hygromycin B was added to initiate antibiotic selection. After 2
579 weeks of culture and passaging, a hygromycin-resistant polyclonal GCaMP6s stable
580 HEK293 cell line was isolated.
581

582 **Plasmid transfection**

583 Wildtype HEK293, GCaMP6s HEK293, Piezo1-KO N2a, and RIN14B cells were used in
584 transfection experiments. Other cell lines were used untransfected to examine
585 endogenously expressed Piezo1 (wildtype N2a cells) or were used in FLIPR
586 experiments described further below (PIEZO1-KO HEK293 cells). Cells were seeded in
587 24-well plates 24 – 72 hours before transfection. Transfection was performed when the
588 cells were at ~70% confluence using 500 ng plasmid DNA and the Lipofectamine 3000
589 kit (Fisher Scientific, L3000001) following the manufacturer's instructions. The following
590 plasmids were used in the study: CMV-mPiezo1-IRES-eGFP, CMV-mPiezo1, and CMV-
591 GCaMP6s. CMV-mPiezo1-IRES-eGFP was a gift from Ardem Patapoutian (Addgene
592 plasmid #80925; http://n2t.net/addgene:80925) and was used for all electrophysiological
593 recordings. CMV-mPiezo1 was previously generated in-house by subcloning mouse
594 Piezo1 into the pcDNA5/FRT expression vector (Fisher Scientific, V601020) – this
595 plasmid was used for all calcium imaging of Piezo1 activity. CMV-GCaMP6s was a gift
596 from Douglas Kim and the GENIE Project (Addgene plasmid #40753;
597 http://n2t.net/addgene:40753) and was used for calcium imaging of RIN14B cells.
598
599 **Calcium imaging**
600 Ringer's solution was used for all physiological assays, consisting of 133 mM NaCl, 3
601 mM KCl, 2.5 mM $CaCl_2$, 1 mM $MgCl_2$, 10 mM glucose, 10 mM HEPES, and 40.9 mM
602 sucrose (all from Sigma-Aldrich) dissolved in water. The pH was adjusted to 7.3 with 1
603 M NaOH and the osmolality was ~330 mmol/kg. Calcium influx was visualized in N2a
604 cells and HEK293 cells using Fluo-4 AM dye (Fisher Scientific, F14201) or the
605 GCaMP6s HEK293 cell line described above. For Fluo-4 AM imaging, 50 µg Fluo-4 AM

606 was dissolved in 44 µL DMSO (Sigma-Aldrich, D2650) and mixed with 9 µL Pluronic F-
607 127 (Fisher Scientific, P-3000MP) by vortexing. 50 µL of this mixture was then diluted in
608 14.3 mL Ringer's solution to make the "loading solution". Cells cultured in 8-chamber
609 slides (Fisher Scientific, 177445PK) were first rinsed with Ringer's solution and then
610 incubated in loading solution for 1 hour light-protected at room temperature. After 1
611 hour, the loading solution was removed, the cells were rinsed with Ringer's solution,
612 and then immediately imaged in Ringer's solution using a pco.panda sCMOS back-
613 illuminated camera at 3 frames per second with an Olympus IX73 inverted microscope
614 and 10x air objective. Videos were recorded and saved using pco.camware software.
615 Solutions containing different compounds were added and removed via micropipette
616 during video recording while maintaining the same volume (150 µL) in the chamber.
617 Stock solutions of all compounds were dissolved and prepared following manufacturer
618 instructions, and the final concentration used in each experiment can be found in each
619 figure legend. The following commercially available compounds were used in the study:
620 ssRNA40 (Invivogen, A40-41-02), ssRNA41 (Invivogen, A41-41-02), Yoda1 (Sigma-
621 Aldrich, SML558-5MG), AITC (Sigma-Aldrich, 377430), gadolinium(III) chloride (Sigma-
622 Aldrich, 439770), A-967979 (Sigma-Aldrich, SML0085), and ionomycin (Sigma-Aldrich,
623 I0634).

624 Fiji software was used to import and analyze video files from pco.camware
625 software (pco). The Template Matching and Slice Alignment plugin was used to align all
626 video frames to correct for any drift (Tseng et al., 2011). For creating still-frame images,
627 a gray-scale baseline image was generated from an average of the first 10 frames of
628 the recording. Separately, a fire-scale standard deviation Z-projection was generated

from the frames where the cells were exposed to a specific treatment. The Z-projection image was then overlaid on top of the gray-scale baseline image to visualize which cells responded to a given treatment. Supplemental videos were made from the raw recordings and exported at 10 frames per second so that 1 second of video is equivalent to 30 seconds of real time.

For quantifying responses, cellular regions of interest (ROIs) were drawn around randomly selected individual cells and used to measure the mean pixel intensity per frame. In cases where only certain regions within the field of view showed calcium influx, such as with poor fluid dispersion or the variable activation seen with fecal/dietary extracts, the ROI selection was restricted to this region of activation. We found that dissolved ssRNA40 and crude extracts produced substantial autofluorescence, which could be a confounding factor when analyzing calcium imaging recordings. However, a standard image background subtraction procedure effectively eliminated most of the fluorescence artifacts. This accomplished by drawing an additional set of 10 background ROIs per recording that were in cell-free areas in the field of view. The mean pixel intensities were exported to Microsoft Excel software for normalization and quantification. An average of the background ROI values was subtracted from each cellular ROI frame-by-frame to correct for artifactual changes in background fluorescence. These values were then used to calculate the $\Delta F/F_0$ for each cell. The mean pixel intensity of the first 10 frames was averaged to yield F_0, and then F_0 was subtracted from each frame's pixel intensity on a frame-by-frame basis to determine ΔF. Dividing ΔF by F_0 ($\Delta F/F_0$) normalized each cell's change in calcium fluorescence to its baseline level of fluorescence.

To quantify the maximal response to different treatments, the peak $\Delta F/F_0$ from within the treatment exposure timeframe was selected for each cell. All recordings ended with ionomycin treatment to elicit maximum calcium influx for normalization purposes. In cases where two different recordings showed significantly different ionomycin responses, the $\Delta F/F_0$ for experimental treatments was normalized a percentage of the peak ionomycin response. $\Delta F/F_0$ values were exported to GraphPad 8.0 (Prism) for visualization and graphing. An n = 25 – 50 cells was analyzed for each calcium imaging recording and are representative of at least 3 independently performed transfections and recording sessions per condition.

Electrophysiology

N2a cells and HEK293 cells were plated in 35 mm dishes (Fisher Scientific, 353001) ~24 hours prior to recording, and the next day they were rinsed once in Ringer's solution before recording in Ringer's solution. Patch clamp recordings were performed in whole-cell voltage-clamp mode by glass micropipette electrodes that were pulled and polished to 2 – 6 MΩ resistance. The pipette was filled with internal solution consisting of 133 mM CsCl, 1 mM $CaCl_2$, 1 mM $MgCl_2$, 5 mM EGTA, 10 mM HEPES, 4 mM Mg-ATP, 0.4 mM Na_2-GTP, 43.8 mM sucrose (all from Sigma-Aldrich). Internal solution pH was adjusted to 7.3 with 1 M CsOH and the osmolality was ~320 mmol/kg. After establishing a GΩ seal with the patch pipette on a cell membrane and breaking into whole-cell configuration, cells were held at -80 mV and mechanically stimulated with a separate glass polished probe to elicit Piezo1 currents. The probe was a micropipette that was heat-polished to seal the tip until rounded with a width of 3 – 5 μm. The probe

675 was attached to a piezoelectric translator (Physik Instrumente, P841.20) and mounted
676 on a micromanipulator (Sutter Instrument, MP-225) at 45º angle to the cell surface. To
677 stimulate the cells, the probe was maneuvered to rest ~1 μm above the cell surface and
678 then sequentially indented for 200 ms in 1 μm increments from 1 – 10 μm with a 2 ms
679 ramp time. Each indentation was separated by 2 seconds. Whole-cell currents were
680 measured by a Multiclamp 700b amplifier (Molecular Devices) and digitized by a
681 Digidata 1550 (Molecular Devices) at 100 kHz and then low-pass filtered at 10 kHz. The
682 signals were saved digitally using Clampex 11.1 software (Molecular Devices).
683 Clampfit 11.1 software (Molecular Devices) was used to analyze the
684 electrophysiological recordings. Any whole-cell recording showing a static leak current >
685 200 pA was discarded from analysis due to poor patch seal quality. Additionally, cells
686 with a peak mechanically evoked current < 30 pA were considered non-responders and
687 discarded, since these currents are near the baseline noise level and their kinetics could
688 not be reliably analyzed. Additionally, cells with a peak current > 4,000 pA were
689 discarded due to the abnormally high values and generally unhealthy swelled
690 morphology of such cells. Finally, recordings were discarded if the patch pipette seal
691 broke before three consecutive mechanically evoked responses, because low
692 indentation responses have distinct kinetics that bias analysis. In the end, an equal
693 number of recordings (5 – 7) were discarded from each condition (from a total of 15 –
694 25 attempted cells/condition), with no apparent systematic bias toward any of the
695 control or ssRNA conditions. The remaining recordings (one per cell) were filtered at 1
696 kHz and thresholded to 0 pA. The maximal current was measured by the largest
697 amplitude response before patch breakage or by reaching 10 μm membrane

indentation, whichever came first. This same response was then used to approximate the time constant of inactivation (tau) by calculating the time taken to decay 63.2% back to baseline. The mechanical activation threshold was determined by the level of membrane indentation (μm) to elicit the first current response peak (pA) above the baseline level of noise. No systematic differences were observed for baseline noise level or maximum membrane indentation between conditions. Values were exported from Clampfit 11.1 to Graphpad 8.0 (Prism) for visualization and graphing. A minimum of n = 7 cells were analyzed per recording condition.

FLIPR assay

PIEZO1-KO HEK293 or wildtype HEK293 cells were grown in Dulbecco's modified Eagle's medium containing 4.5 mg/ml glucose, 10% fetal bovine serum, and 1x pen/strep. Cells were plated in 6-well plates and transfected using Lipofectamine 2000 (ThermoFisher Scientific), according to the manufacturer's instructions. Human PIEZO1 fused to IRES-TdTomato or mouse Piezo1 fused to IRES-GFP was transfected at 2 μg per well (6-well plate) for fluorescent imaging plate reader (FLIPR). One day after transfection, the cells were dissociated from 6-well plates with trypsin and re-seeded into a 384-well plate, at 20,000 cells per well. The plate was then cultured for 1 day before washing with assay buffer (1x HBSS, 10 mM HEPES, pH 7.4) in a ELx405 CW plate washer (BioTek Instruments). The cells were then incubated with 1.25 μM calcium indicator Fluo-8 AM (AAT Bioquest) in the assay buffer at 37 C for 1 hour. After washing out excess dye, fluorescence was measured on a fluorescent imaging plate reader (FLIPR) Tetra upon treatment with various reagents. A 1 mM stock solution of Yoda1 in

721 dimethyl sulfoxide (DMSO) was used resulting in a final concentration of 5 μM Yoda1
722 and 0.5% DMSO in the assay. The effect of ssRNA40 was tested at concentrations of 5,
723 2.5, 1.25, 0.625 μg/ml. Ionomycin was added to 10 μM concentration as a final
724 normalization. All measurements were taken from 4 biological replicates (4 different
725 wells in 384-well plate).
726
727 **Crude extract preparations**
728 Fresh mouse feces were gathered by gently holding the mouse over a sterile 1.5 mL
729 tube and collecting the fecal matter directly into the tube as it was excreted. Feces from
730 10 – 20 adult mice were pooled together, diluted to 0.1 g/mL in Ringer's solution, and
731 homogenized using a sterile mortar and pestle. The sample was then centrifuged at 300
732 rcf for 3 minutes to pellet any remaining undissolved fecal matter and then sequentially
733 filtered through 100, 40, and finally 0.45 μm mesh membranes (Fisher Scientific,
734 SLHAR33SS) to produce the "fecal extract". Because this extract was strongly
735 autofluorescent during calcium imaging, the fecal extract was further diluted 1:20 in
736 Ringer's solution from its original 0.1 g/mL to a final concentration of 5 mg/mL when
737 applying it to cell cultures. Dietary extracts were prepared in identical fashion to fecal
738 extracts, with the exception that mouse food pellets were first crushed in a dry state
739 using mortar and pestle and then transferred to Ringer's solution (0.1 g/mL).
740 Four different fecal extract preparations and three different dietary extract
741 preparations were independently made and tested over the course of the study at the
742 NIH. A separate set of fecal and dietary extracts were prepared from mice at
743 Scripps/HHMI. The NIH-sourced extracts showed substantially more stimulatory activity

on HEK293 cells when tested in parallel with the Scripps/HHMI extracts, indicating possible differences owing to the specific mouse colony and commercial diet source. For RNase treatment of fecal extracts, RNase A (Fisher Scientific, EN0531) was added at a final concentration of 500 µg/mL to the 0.1 g/mL fecal extract and incubated at 37 ºC for 30 minutes. Mock-treated fecal extracts were handled in the same way but without addition of RNase A. The RNase- and mock-treated fecal extracts were then used for calcium imaging on Piezo1-transfected HEK293 cells at a final concentration of 5 mg feces per mL.

To ensure that the fecal and dietary extracts were not nonspecifically activating cells due to changes in osmolality or pH, these properties were examined in extracts that were diluted to the working concentration of 5 mg/mL in Ringer's solution. The control Ringer's solution that was tested had an osmolality of ~336 mmol/kg and 7.5 pH. In comparison, fecal extract was ~332 mmol/kg and 7.5 pH, and dietary extract was ~334 mmol/kg and 7.5 pH. These measurements indicate that the extracts did not substantially affect the osmolality or pH of the solutions.

Fecal RNA purification

RNA was extracted from mouse feces by a standard phenol/chloroform protocol. 500 µL TRIzol (Fisher Scientific, 15596026) was added per 50 mg feces and then homogenized using an RNase-free tube and plunger (Takara, 9791A). 100 µL chloroform (Sigma-Aldrich) was then added per 500 µL TRIzol, vortexed vigorously followed by 3 minute incubation at room temperature, and then centrifuged at 12,000 rcf for 10 minutes at 4 ºC. The aqueous layer was transferred to a clean tube and the RNA was extracted

767 using the miRNeasy kit (Qiagen, 217004) following manufacturer's instructions. The
768 RNA content of the samples was measured using a NanoDrop (Fisher Scientific, ND-
769 2000), confirming a ~2.0 ratio of 260/280 nm absorbance. These purified RNA samples
770 yielded ~ 300 ng/µL RNA, while RNA in the crude fecal extracts was below the
771 detection range of the NanoDrop. The samples were separated on an agarose gel and
772 examined for nucleic acid content. The purified fecal RNA manifested as a smear,
773 ranging from short oligonucleotides tens of base pairs (bp) in size up to 300 bp (Figure
774 3C). To confirm that the samples were in fact RNA and not DNA, fecal extracts and
775 purified fecal RNA were treated with 500 µg/mL RNase A (Fisher Scientific, EN0531) for
776 30 minutes at 37 ºC before running on an agarose gel (Figure 3C). The fecal RNA was
777 then tested on Piezo1-transfected HEK293 cells at a final concentration of 10 µg/mL,
778 which was the same concentration used in the Sugisawa study (Figure 3D).

779 Additionally, fecal RNA was purified using the same methodology and
780 Nucleospin Triprep kit (Macherey-Nagel, 740966.10) as in the Sugisawa study,
781 following the manufacturer's instructions. 350 µL buffer RP1 was added per 50 mg
782 feces, and the samples were homogenized using an RNase-free tube and plunger
783 (Takara, 9791A) and then vortexed for 5 seconds. A wide-bore pipette was then used to
784 transfer the samples to a Nucleospin filter, and the RNA was washed and extracted
785 following the Triprep protocol. RNA concentration was 100 – 200 ng/µL and the purity
786 was confirmed by a ~2.0 ratio of 260/280 nm absorbance via NanoDrop. Applying these
787 purified fecal RNA samples at a final concentration of 10 µg/mL did not elicit calcium
788 influx in Piezo1-transfected HEK293 cells.

789

Single-nuclei RNA sequencing

RIN14B cells were put on ice, washed with chilled PBS, and then lysed with chilled Nuclei EZ lysis buffer (Sigma-Aldrich, NUC-101). Single cells were isolated with a 40 µm filter and pelleted in a centrifuge for 8 minutes, 800 rcf, 4 °C. The nuclei were resuspended using PBS with 1% BSA and counted using a hemocytometer with trypan blue viability dye. The nuclei were centrifuged and resuspended at an appropriate volume for the 10X Chromium system (10X Genomics). The nuclei were counted once more to check the number and quality before proceeding with 10X Chromium processing and library construction as per the manufacturer's instructions. Next Gen sequencing with a Chromium V2 chemistry was carried out on an Illumina NextSeq 500. Illumina NextSeq 500 pre-mRNA sequencing data were aligned to the *rattus norvegicus* genome using CellRanger. The data were then analyzed with Seurat V3.0 as described previously (Butler et al., 2018).

Statistical analysis

All data were first tested for normality using the Shapiro-Wilk test. Normally distributed data were analyzed by one-way ANOVA with Bonferroni multiple comparisons correction, and non-normally distributed data were analyzed by Kruskal Wallis test with Dunn's multiple comparisons correction. Statistical significance was determined by a p value less than 0.05. The degree of statistical significance is indicated in each figure legend using asterisks. 1 cell equals 1 biological replicate for calcium imaging and electrophysiology experiments. The n number of biological replicates for each condition are representative of at least 3 separately run experiments. The n and error bar

definitions are reported in each figure legend. No power analyses were done to determine sample sizes *a priori*, but our sample sizes adhere to those reported in similar previous studies (Sugisawa et al., 2020). All graphing and statistical testing was performed in GraphPad 8.0 software (Prism) and figures were assembled in Adobe Illustrator 2021.

Data availability

The single-nuclei RNA sequencing data of the RIN14B cell line have been deposited in the Gene Expression Omnibus (GEO) database under accession number GSE213903. It can be accessed while it remains in private status using the following secure token: izkjgeiwjtgdheh.

REFERENCES

Albuisson, J., Murthy, S.E., Bandell, M., Coste, B., Louis-Dit-Picard, H., Mathur, J., Fénéant-Thibault, M., Tertian, G., De Jaureguiberry, J.P., Syfuss, P.Y., et al. (2013). Dehydrated hereditary stomatocytosis linked to gain-of-function mutations in mechanically activated PIEZO1 ion channels. Nat. Commun. *4*, 1884.

Bae, C., Gnanasambandam, R., Nicolai, C., Sachs, F., and Gottlieb, P.A. (2013). Xerocytosis is caused by mutations that alter the kinetics of the mechanosensitive channel PIEZO1. Proc. Natl. Acad. Sci. U. S. A. *110*, E1162–E1168.

Bellono, N.W., Bayrer, J.R., Leitch, D.B., Castro, J., Zhang, C., O'Donnell, T.A., Brierley, S.M., Ingraham, H.A., and Julius, D. (2017). Enterochromaffin Cells Are Gut Chemosensors that Couple to Sensory Neural Pathways. Cell *170*, 185-198.e16.

Borbiro, I., Badheka, D., and Rohacs, T. (2015). Activation of TRPV1 channels inhibits mechanosensitive Piezo channel activity by depleting membrane phosphoinositides. Sci. Signal. *8*, ra15.

Botello-smith, W.M., Jiang, W., Lacroix, J.J., and Luo, Y. (2019). A mechanism for the activation of the mechanosensitive Piezo1 channel by the small molecule Yoda1. Nat. Commun. *10*, 4503.

Butler, A., Hoffman, P., Smibert, P., Papalexi, E., and Satija, R. (2018). Integrating single-cell transcriptomic data across different conditions, technologies, and species. Nat. Biotechnol. *36*, 411–420.

Cahalan, S.M., Lukacs, V., Ranade, S.S., Chien, S., Bandell, M., and Patapoutian, A. (2015). Piezo1 links mechanical forces to red blood cell volume. Elife *4*, e07370.

Chesler, A.T., Szczot, M., Bharucha-Goebel, D., Čeko, M., Donkervoort, S., Laubacher, C., Hayes, L.H., Alter, K., Zampieri, C., Stanley, C., et al. (2016). The Role of PIEZO2 in Human Mechanosensation. N. Engl. J. Med. *375*, 1355–1364.

Chiu, I.M., Barrett, L.B., Williams, E.K., Strochlic, D.E., Lee, S., Weyer, A.D., Lou, S., Bryman, G.S., Roberson, D.P., Ghasemlou, N., et al. (2014). Transcriptional profiling at whole population and single cell levels reveals somatosensory neuron molecular diversity. Elife *3*, e04660.

Cinar, E., Zhou, S., Decourcey, J., Wang, Y., Waugh, R.E., and Wan, J. (2015). Piezo1 regulates mechanotransductive release of ATP from human RBCs. Proc. Natl. Acad. Sci. U. S. A. *112*, 11783–11788.

Coste, B., Mathur, J., Schmidt, M., Earley, T.J., Ranade, S., Petrus, M.J., Dubin, A.E., and Patapoutian, A. (2010). Piezo1 and Piezo2 Are Essential Components of Distinct Mechanically Activated Cation Channels. Science (80-.). *330*, 55–60.

Dubin, A.E., Schmidt, M., Mathur, J., Petrus, M.J., Xiao, B., Coste, B., and Patapoutian, A. (2012). Inflammatory Signals Enhance Piezo2-Mediated Mechanosensitive Currents. Cell Rep. *2*, 511–517.

Dubin, A.E., Murthy, S., Lewis, A.H., Brosse, L., Cahalan, S.M., Grandl, J., Coste, B., and Patapoutian, A. (2017). Endogenous Piezo1 Can Confound Mechanically Activated Channel Identification and Characterization. Neuron *94*, 266–270.

Eisenhoffer, G.T., Loftus, P.D., Yoshigi, M., Otsuna, H., Chien, C. Bin, Morcos, P.A., and Rosenblatt, J. (2012). Crowding induces live cell extrusion to maintain homeostatic cell numbers in epithelia. Nature *484*, 546–549.

Faucherre, A., Kissa, K., Nargeot, J., Mangoni, M.E., and Jopling, C. (2014). Piezo1

873 plays a role in erythrocyte volume homeostasis. Haematologica *99*, 70–75.

874 Fotiou, E., Martin-Almedina, S., Simpson, M.A., Lin, S., Gordon, K., Brice, G., Atton, G.,

875 Jeffery, I., Rees, D.C., Mignot, C., et al. (2015). Novel mutations in PIEZO1 cause an

876 autosomal recessive generalized lymphatic dysplasia with non-immune hydrops fetalis.

877 Nat. Commun. *6*, 8085.

878 Gaub, B.M., and Müller, D.J. (2017). Mechanical Stimulation of Piezo1 Receptors

879 Depends on Extracellular Matrix Proteins and Directionality of Force. Nano Lett. *17*,

880 2064–2072.

881 Geng, J., Liu, W., Zhou, H., Zhang, T., Wang, L., Zhang, M., Li, Y., Shen, B., Li, X., and

882 Xiao, B. (2020). A Plug-and-Latch Mechanism for Gating the Mechanosensitive Piezo

883 Channel. Neuron *106*, 438-451.e6.

884 Glogowska, E., Schneider, E.R., Maksimova, Y., Schulz, V.P., Lezon-Geyda, K., Wu, J.,

885 Radhakrishnan, K., Keel, S.B., Mahoney, D., Freidmann, A.M., et al. (2017). Novel

886 mechanisms of PIEZO1 dysfunction in hereditary xerocytosis. Blood *130*, 1845–1856.

887 Heil, F., Hemmi, H., Hochrein, H., Ampenberger, F., Kirschning, C., Akira, S., Lipford,

888 G., Wagner, H., and Bauer, S. (2004). Species-Specific Recognition of Single-Stranded

889 RNA via Toll-like Receptor 7 and 8. Science (80-.). *303*, 1526–1530.

890 Hendrickx, G., Fischer, V., Liedert, A., von Kroge, S., Haffner-Luntzer, M., Brylka, L.,

891 Pawlus, E., Schweizer, M., Yorgan, T., Baranowsky, A., et al. (2021). Piezo1

892 Inactivation in Chondrocytes Impairs Trabecular Bone Formation. J. Bone Miner. Res.

893 *36*, 369–384.

894 Jiang, F., Yin, K., Wu, K., Zhang, M., Wang, S., Cheng, H., Zhou, Z., and Xiao, B.

895 (2021). The mechanosensitive Piezo1 channel mediates heart mechano-chemo

transduction. Nat. Commun. *12*, 869.

Kupari, J., Häring, M., Agirre, E., Castelo-Branco, G., and Ernfors, P. (2019). An Atlas of Vagal Sensory Neurons and Their Molecular Specialization. Cell Rep. 2508–2523.

Lee, W., Leddy, H.A., Chen, Y., Lee, S.H., Zelenski, N.A., McNulty, A.L., Wu, J., Beicker, K.N., Coles, J., Zauscher, S., et al. (2014). Synergy between Piezo1 and Piezo2 channels confers high-strain mechanosensitivity to articular cartilage. Proc. Natl. Acad. Sci. U. S. A. *111*, E5114–E5122.

Lehmann, S.M., Rosenberger, K., Krüger, C., Habbel, P., Derkow, K., Kaul, D., Rybak, A., Brandt, C., Schott, E., Wulczyn, F.G., et al. (2012). Extracellularly Delivered Single-Stranded Viral RNA Causes Neurodegeneration Dependent on TLR7. J. Immunol. *189*, 1448–1458.

Li, J., Hou, B., Tumova, S., Muraki, K., Bruns, A., Ludlow, M.J., Sedo, A., Hyman, A.J., McKeown, L., Young, R.S., et al. (2014). Piezo1 integration of vascular architecture with physiological force. Nature *515*, 279–282.

Li, X., Han, L., Nookaew, I., Mannen, E., Silva, M.J., Almeida, M., and Xiong, J. (2019). Stimulation of Piezo1 by mechanical signals promotes bone anabolism. Elife *8*, e49631.

Liu, T., Du, X., Zhang, B., Zi, H., Yan, Y., Yin, J., Hou, H., Gu, S., Chen, Q., and Du, J. (2020). Piezo1-Mediated Ca2+ Activities Regulate Brain Vascular Pathfinding during Development. Neuron *108*, 180–192.

Lukacs, V., Mathur, J., Mao, R., Bayrak-Toydemir, P., Procter, M., Cahalan, S.M., Kim, H.J., Bandell, M., Longo, N., Day, R.W., et al. (2015). Impaired PIEZO1 function in patients with a novel autosomal recessive congenital lymphatic dysplasia. Nat. Commun. *6*, 8329.

Martins, J.R., Penton, D., Peyronnet, R., Arhatte, M., Moro, C., Picard, N., Kurt, B., Patel, A., Honoré, E., and Demolombe, S. (2016). Piezo1-dependent regulation of urinary osmolarity. Pflugers Arch. Eur. J. Physiol. *468*, 1197–1206.

Miyamoto, T., Mochizuki, T., Nakagomi, H., Kira, S., Watanabe, M., Takayama, Y., Suzuki, Y., Koizumi, S., Takeda, M., and Tominaga, M. (2014). Functional role for Piezo1 in stretch-evoked Ca2+ influx and ATP release in Urothelial cell cultures. J. Biol. Chem. *289*, 16565–16575.

Moroni, M., Servin-Vences, M.R., Fleischer, R., Sánchez-Carranza, O., and Lewin, G.R. (2018). Voltage gating of mechanosensitive PIEZO channels. Nat. Commun. *9*, 1096.

Murthy, S.E., Dubin, A.E., and Patapoutian, A. (2017). Piezos thrive under pressure: mechanically activated ion channels in health and disease. Nat. Rev. Mol. Cell Biol.

Narayanan, P., Hütte, M., Kudryasheva, G., Taberner, F.J., Lechner, S.G., Rehfeldt, F., Gomez-Varela, D., and Schmidt, M. (2018). Myotubularin related protein-2 and its phospholipid substrate PIP2 control Piezo2-mediated mechanotransduction in peripheral sensory neurons. Elife *7*, e32346.

Nguyen, M.Q., Wu, Y., Bonilla, L.S., von Buchholtz, L.J., and Ryba, N.J.P. (2017). Diversity amongst trigeminal neurons revealed by high throughput single cell sequencing. PLoS One *12*, e0185543.

Nonomura, K., Lukacs, V., Sweet, D.T., Goddard, L.M., Kanie, A., Whitwam, T., Ranade, S.S., Fujimori, T., Kahn, M.L., and Patapoutian, A. (2018). Mechanically activated ion channel PIEZO1 is required for lymphatic valve formation. Proc. Natl. Acad. Sci. U. S. A. *115*, 12817–12822.

Nozawa, K., Kawabata-Shoda, E., Doihara, H., Kojima, R., Okada, H., Mochizuki, S.,

942 Sano, Y., Inamura, K., Matsushime, H., Koizumi, T., et al. (2009). TRPA1 regulates
943 gastrointestinal motility through serotonin release from enterochromaffin cells. Proc.
944 Natl. Acad. Sci. U. S. A. *106*, 3408–3413.
945 Park, C.K., Xu, Z.Z., Berta, T., Han, Q., Chen, G., Liu, X.J., and Ji, R.R. (2014).
946 Extracellular microRNAs Activate nociceptor neurons to elicit pain via TLR7 and
947 TRPA1. Neuron *82*, 47–54.
948 Pathak, M.M., Nourse, J.L., Tran, T., Hwe, J., Arulmoli, J., Le, D.T.T., Bernardis, E.,
949 Flanagan, L.A., and Tombola, F. (2014). Stretch-activated ion channel Piezo1 directs
950 lineage choice in human neural stem cells. Proc. Natl. Acad. Sci. U. S. A. *111*, 16148–
951 16153.
952 Ranade, S., Woo, S., Dubin, A., Moshourab, R., Wetzel, C., Petrus, M., Mathur, J.,
953 Bégay, V., Coste, B., Mainquist, J., et al. (2014a). Piezo2 is the major transducer of
954 mechanical forces for touch sensation in mice. Nature *516*, 121–125.
955 Ranade, S.S., Qiu, Z., Woo, S.H., Hur, S.S., Murthy, S.E., Cahalan, S.M., Xu, J.,
956 Mathur, J., Bandell, M., Coste, B., et al. (2014b). Piezo1, a mechanically activated ion
957 channel, is required for vascular development in mice. Proc. Natl. Acad. Sci. U. S. A.
958 *111*, 10347–10352.
959 Retailleau, K., Duprat, F., Arhatte, M., Ranade, S.S., Peyronnet, R., Martins, J.R.,
960 Jodar, M., Moro, C., Offermanns, S., Feng, Y., et al. (2015). Piezo1 in Smooth Muscle
961 Cells Is Involved in Hypertension-Dependent Arterial Remodeling. Cell Rep. *13*, 1161–
962 1171.
963 Ridone, P., Vassalli, M., and Martinac, B. (2019). Piezo1 mechanosensitive channels:
964 what are they and why are they important. Biophys. Rev. *11*, 795–805.

965 Ridone, P., Pandzic, E., Vassalli, M., Cox, C.D., Macmillan, A., Gottlieb, P.A., and
966 Martinac, B. (2020). Disruption of membrane cholesterol organization impairs the
967 activity of PIEZO1 channel clusters. J. Gen. Physiol. *152*, e201912515.
968 Rode, B., Shi, J., Endesh, N., Drinkhill, M.J., Webster, P.J., Lotteau, S.J., Bailey, M.A.,
969 Yuldasheva, N.Y., Ludlow, M.J., Cubbon, R.M., et al. (2017). Piezo1 channels sense
970 whole body physical activity to reset cardiovascular homeostasis and enhance
971 performance. Nat. Commun. *8*, 350.
972 Romero, L.O., Massey, A.E., Mata-Daboin, A.D., Sierra-Valdez, F.J., Chauhan, S.C.,
973 Cordero-Morales, J.F., and Vásquez, V. (2019). Dietary fatty acids fine-tune Piezo1
974 mechanical response. Nat. Commun. *10*, 1200.
975 Romero, L.O., Caires, R., Nickolls, A.R., Chesler, A.T., Cordero-Morales, J.F., and
976 Vasques, V. (2020). A dietary fatty acid counteracts neuronal mechanical sensitization.
977 Nat. Commun. 2997.
978 Shibata, T., Ohto, U., Nomura, S., Kibata, K., Motoi, Y., Zhang, Y., Murakami, Y., Fukui,
979 R., Ishimoto, T., Sano, S., et al. (2016). Guanosine and its modified derivatives are
980 endogenous ligands for TLR7. Int. Immunol. *28*, 211–222.
981 Solis, A.G., Bielecki, P., Steach, H.R., Sharma, L., Harman, C.C.D., Yun, S., de Zoete,
982 M.R., Warnock, J.N., To, S.D.F., York, A.G., et al. (2019). Mechanosensation of cyclical
983 force by PIEZO1 is essential for innate immunity. Nature *573*, 69–74.
984 Sugimoto, A., Miyazaki, A., Kawarabayashi, K., Shono, M., Akazawa, Y., Hasegawa, T.,
985 Ueda-Yamaguchi, K., Kitamura, T., Yoshizaki, K., Fukumoto, S., et al. (2017). Piezo
986 type mechanosensitive ion channel component 1 functions as a regulator of the cell fate
987 determination of mesenchymal stem cells. Sci. Rep. *7*, 17696.

988 Sugisawa, E., Takayama, Y., Takemura, N., Sunagawa, M., Sugisawa, E., Takayama,
989 Y., Takemura, N., Kondo, T., and Hatakeyama, S. (2020). RNA Sensing by Gut Piezo1
990 Is Essential for Systemic Serotonin Synthesis. Cell *182*, 609–624.
991 Sun, W., Chi, S., Li, Y., Ling, S., Tan, Y., Xu, Y., Jiang, F., Li, J., Liu, C., Zhong, G., et
992 al. (2019). The mechanosensitive Piezo1 channel is required for bone formation. Elife *8*,
993 e47454.
994 Syeda, R. (2021). Physiology and Pathophysiology of Mechanically Activated PIEZO
995 Channels. Annu. Rev. Neurosci. *44*, 383–402.
996 Syeda, R., Xu, J., Dubin, A.E., Coste, B., Mathur, J., Huynh, T., Matzen, J., Lao, J.,
997 Tully, D.C., Engels, I.H., et al. (2015). Chemical activation of the mechanotransduction
998 channel Piezo1. Elife *4*, e07369.
999 Szczot, M., Nickolls, A.R., Lam, R.M., and Chesler, A.T. (2021). The Form and Function
1000 of PIEZO2. Annu. Rev. Biochem. *90*, 507–534.
1001 Tseng, Q., Wang, I., Duchemin-Pelletier, E., Azioune, A., Carpi, N., Gao, J., Filhol, O.,
1002 Piel, M., Théry, M., and Balland, M. (2011). A new micropatterning method of soft
1003 substrates reveals that different tumorigenic signals can promote or reduce cell
1004 contraction levels. Lab Chip *11*, 2231–2240.
1005 Usoskin, D., Furlan, A., Islam, S., Abdo, H., Lönnerberg, P., Lou, D., Hjerling-Leffler, J.,
1006 Haeggström, J., Kharchenko, O., Kharchenko, P. V., et al. (2015). Unbiased
1007 classification of sensory neuron types by large-scale single-cell RNA sequencing. Nat.
1008 Neurosci. *18*, 145–153.
1009 Wang, F., Knutson, K., Alcaino, C., Linden, D.R., Gibbons, S.J., Kashyap, P., Grover,
1010 M., Oeckler, R., Gottlieb, P.A., Li, H.J., et al. (2017). Mechanosensitive ion channel

1011 Piezo2 is important for enterochromaffin cell response to mechanical forces. J. Physiol.
1012 *595*, 79–91.
1013 Wang, L., You, X., Lotinun, S., Zhang, L., Wu, N., and Zou, W. (2020). Mechanical
1014 sensing protein PIEZO1 regulates bone homeostasis via osteoblast-osteoclast
1015 crosstalk. Nat. Commun. *11*, 282.
1016 Wang, S.P., Chennupati, R., Kaur, H., Iring, A., Wettschureck, N., and Offermanns, S.
1017 (2016). Endothelial cation channel PIEZO1 controls blood pressure by mediating flow-
1018 induced ATP release. J. Clin. Invest. *126*, 4527–4536.
1019 Wang, Y., Chi, S., Guo, H., Li, G., Wang, L., Zhao, Q., Rao, Y., Zu, L., He, W., and
1020 Xiao, B. (2018). A lever-like transduction pathway for long-distance chemical- and
1021 mechano-gating of the mechanosensitive Piezo1 channel. Nat. Commun. *9*, 1300.
1022 Woo, S.H., Ranade, S., Weyer, A.D., Dubin, A.E., Baba, Y., Qiu, Z., Petrus, M.,
1023 Miyamoto, T., Reddy, K., Lumpkin, E.A., et al. (2014). Piezo2 is required for Merkel-cell
1024 mechanotransduction. Nature *509*, 622–626.
1025 Woo, S.H., Lukacs, V., Nooij, J.C. de, Zaytseva, D., Criddle, C.R., Francisco, A.,
1026 Jessell, T.M., Wilkinson, K.A., and Patapoutian, A. (2015). Piezo2 is the principal
1027 mechanotransduction channel for proprioception. Nat. Neurosci. *18*, 1756–1762.
1028 Zhang, Z., Ohto, U., Shibata, T., Taoka, M., Yamauchi, Y., Sato, R., Shukla, N.M.,
1029 David, S.A., Isobe, T., Miyake, K., et al. (2018). Structural Analyses of Toll-like Receptor
1030 7 Reveal Detailed RNA Sequence Specificity and Recognition Mechanism of Agonistic
1031 Ligands. Cell Rep. *25*, 3371–3381.
1032 Zhao, Q., Zhou, H., Li, X., and Xiao, B. (2019). The mechanosensitive Piezo1 channel:
1033 a three-bladed propeller-like structure and a lever-like mechanogating mechanism.

1034 FEBS J. *286*, 2461–2470.

1035 Zhou, T., Gao, B., Fan, Y., Liu, Y., Feng, S., Cong, Q., Zhang, X., Zhou, Y., Yadav,

1036 P.S., Lin, J., et al. (2020). Piezo1/2 mediate mechanotransduction essential for bone

1037 formation through concerted activation of NFAT-YAP1-β-catenin. Elife *9*, e52779.

1038

1039